CHARACTERIZATION OF SEGMENTATION AND LONG-TERM VERTICAL SLIP RATES OF THE WASATCH FAULT ZONE, UTAH

by

Julia Corbett Howe

A thesis submitted to the faculty of
The University of Utah
in partial fulfillment of the requirements for the degree of

Master of Science

in

Geological Engineering

Department of Geology and Geophysics

The University of Utah

August 2017

The University of Utah Graduate School

STATEMENT OF THESIS APPROVAL

The thesis of **Julia Corbett Howe**

has been approved by the following supervisory committee members:

Paul Jewell	, Chair	**4/14/2017** Date Approved
Ronald Bruhn	, Member	**4/14/2017** Date Approved
Peter Lippert	, Member	**4/14/2017** Date Approved

and by **Thure Cerling**, Chair/Dean of

the Department/College/School of **Geology and Geophysics**

and by David B. Kieda, Dean of The Graduate School.

ABSTRACT

The segmentation model of the Wasatch Fault Zone (WFZ) in north-central Utah has been central to understanding normal fault systems around the world. In this study, we test the notion that the classically defined Brigham City-Weber segment boundary is a barrier to earthquake rupture. To do this, we examined the elevation change of the Bonneville and Provo highstand shorelines of Lake Bonneville along these fault segments. We measured shoreline paleoelevation using the publicly available ± 20 cm vertical accuracy light detection and ranging (lidar) dataset sponsored by the State of Utah (2013-2014) and a new ArcGIS toolbox called PaleoElev that was developed as part of this study.

Elevation profiles of the Bonneville and Provo shorelines along the footwall of the fault exhibit constant elevation from the southern end of the Weber segment to the northern subsegment of the Brigham City segment. These elevation patterns suggest that the southern subsegment of the Brigham City segment is linked to the Weber segment and has commonly ruptured coseismically with the Weber segment since the late Pleistocene. The northern subsegment of the Brigham City segment exhibits little to no elevation change, and it is unclear as to whether this subsegment has been active since the late Pleistocene.

Where the shorelines are displaced by the WFZ, we have calculated vertical slip rates. The vertical slip rates calculated in this study have significant uncertainty

associated with the shoreline paleoelevation measurements. We can only confidently report two vertical slip rates from the Provo shoreline at the Pleasant View Salient, which correlate well to Holocene rates calculated from paleoseismic trenching data and support our interpretation that the Pleasant View Salient is not a barrier to fault rupture.

TABLE OF CONTENTS

LIST OF TABLES

Tables

ACKNOWLEDGEMENTS

This thesis represents the combined ideas and efforts of the many bright minds I have been fortunate enough to collaborate with during my time in Utah, and without whom my success in graduate school would never have been possible. First and foremost, I would like to thank my advisor Paul Jewell for allowing me to pursue my numerous ideas throughout the course of this project – even when the success of my endeavors seemed tenuous. Thank you for providing insight into the dynamic Lake Bonneville and helping me work through the complicated role its shorelines have had in this project.

I would also like to thank my committee member Ron Bruhn for taking time out of retirement to guide me throughout this project: sending emails from the marina between sailing stints, returning to Salt Lake to teach me the important “shoreline or fault scarp” distinction in the field, and providing insight to the mechanics of the Wasatch Fault. To my committee member Pete Lippert, thank you for always sharing sound ideas and advice. From encouraging a conversation with a Distinguished Lecture Series (DLS) speaker that changed the course of this project to recommending short courses at University NAVSTAR Consortium (UNAVCO), your suggestions have always pushed me in a positive direction. Jim Pechmann, thank you for always having an idea (or three) on how to keep improving the quality of my work.

I would also like to acknowledge my contacts at the Utah Geological Survey, who have been instrumental in my understanding of Utah geology. Adam McKean, thank you

for meeting with me throughout the course of this project to discuss geomorphology and geology along the Wasatch Front, and patiently answering countless out-of-context emails. To Emily Kleber, thank you for sharing ideas, contacts, and encouraging me not to settle for anything less than I am capable of. It is a powerful thing to have a female role model in this field.

I would also like to thank the organizations that have provided funding for this project: the National Earthquake Hazards Reduction Program (NEHRP), the University of Utah Global Change and Sustainability Center (GCSC), and the Geological Society of America Environmental and Engineering Geology Division (GSA EEGD). This funding has not only allowed me to focus my energy on the research presented in this thesis, but to collaborate with people I would otherwise never have had the opportunity to meet. Thank you also to Ken Adams for providing the data needed to perform the isostatic corrections in this study.

On a more personal note, I would like to thank my friends and family for their unwavering emotional and, at times, literally physical support for the last 2 years. To my friends – there are too many of you to thank individually, but I can thank each and every one of you for much needed nights out and listening to my never-ending stories about knees and shorelines. To my parents, my success in this program is only possible because of your support. Thank you for encouraging me to pursue science (even though I am really an artist), for long phone conversations every Sunday, and for not dragging me back to South Carolina after I broke my leg. Sticking it out in Utah was the right choice for me, if a tough one on all of us.

Finally, I would like to thank my boyfriend Josh Nolin for being my rock every

step of the way (several puns intended). Thank you for sticking around and doing my grocery shopping when I could not walk, and for always understanding the late nights and early mornings spent working towards this degree. More importantly, thank you for providing the laughs and adventures that made these years in Utah the best years yet.

INTRODUCTION

The growing availability of high-resolution light detection and ranging (lidar) data has created the potential to measure surface topography in great detail. Of particular interest are geomorphological features such as shorelines and marine terraces that preserve a record of fault activity in tectonically active regions. The Bonneville and Provo shoreline highstands of late Pleistocene Lake Bonneville are prime examples of potential tectonic markers: they are laterally continuous, well age-constrained, and in close proximity to the Wasatch Fault Zone (WFZ). These features can be measured in detail using a publicly available lidar dataset sponsored by the State of Utah in 2013-2014 (http://gis.utah.gov/data). This high-resolution lidar dataset, with 0.5 m horizontal and ± 20 cm vertical accuracy, covers the extent of the WFZ and many proximal Bonneville and Provo shorelines within the state of Utah.

Shoreline paleoelevation needed to accurately interpret neotectonic deformation is not always straightforward to measure, however. Many Pleistocene and Holocene shorelines have been subject to surface processes that make surface elevation a poor approximation of paleoelevation. Even the most well-preserved Lake Bonneville shorelines have developed colluvial wedges on their shoreline benches as a result of landscape diffusion. In this study, we present a new ArcGIS toolbox named PaleoElev that automates paleoelevation approximation based on the methods presented by Jewell and Bruhn (2013). We apply the PaleoElev tool to Lake Bonneville shorelines in order to

interpret the temporal and spatial rupture patterns of the Brigham City and Weber segments of the WFZ since the late Pleistocene.

Lake Bonneville

Lake Bonneville was the largest pluvial lake located in the Great Basin of western North America during the late Pleistocene (Figure 1). Fluctuating lake levels through time (Figure 2) formed both constructional and erosional landforms during the respective transgressive and regressive phases of the lake's history. These features have been used in interpretations of paleoclimate (Currey, 1990; Oviatt *et al.*, 1992), isostatic reconstructions (Gilbert, 1890; Currey, 1982; Bills *et al.*, 2002; Adams and Bills, 2016; Chen and Maloof, 2017), lithosphere and mantle characterization (Bills and May, 1987), and more recently, neotectonic analysis (Jewell and Bruhn, 2013).

Although both constructional and erosional landforms have been analyzed in these and other studies, erosional shoreline terraces have long been considered more robust indicators of still-water lake elevation than their depositional counterparts (Johnson, 1933; Miller, 1939). The most prominent and easily correlated of these shoreline landforms are the Bonneville, Provo, and Stansbury shorelines first identified by G.K. Gilbert (1890). This study focuses on the Bonneville and Provo shorelines.

Characterization of Bonneville and Provo shorelines. The Bonneville shoreline was first recognized, named, and described by Gilbert (1890). Gilbert postulated that the lake never stabilized at the Bonneville highstand, but began to overflow as soon as it reached the basin low-point at Red Rock Pass and catastrophically flooded into the Snake River basin almost immediately thereafter. Later investigations of the Bonneville

shoreline classified it as an erosional shoreline that briefly stabilized at its highstand before the flood. This characterization prevailed over Gilbert's original interpretation throughout much of the published literature (Oviatt and Jewell, 2016).

Recently, Oviatt and Jewell (2016) have revisited Gilbert's original interpretation of the shoreline. They suggest that as the lake transgressed to the 18 ky Bonneville level (Oviatt, 2015), it deposited the material that it eroded from the basin walls onto its own shoreline platforms (Figure 3). This material was never eroded away because the lake never stabilized at its highstand, and therefore, the Bonneville shoreline should be reclassified as a depositional terrace (Oviatt and Jewell, 2016). The Provo shoreline, in contrast, represents a stable lake level that formed between 15-18 ky (Oviatt, 2015) following the Bonneville flood. Due to stable nature of the lake level over the course of 3 ky, the wave cut platforms of the Provo shorelines are well-developed and considered to be true erosional terraces (Godsey *et al.*, 2005, 2011) (Figure 3).

Isostatic rebound. The shorelines of Lake Bonneville were approximately horizontal at their formation. Any subsequent change in shoreline elevation is a record of surface deformation, which for the Bonneville and Provo shorelines is caused primarily by isostatic rebound and tectonic activity. Isostatic rebound of the shorelines was first recognized by G.K. Gilbert (1890), who observed that the shorelines were characterized by a domal deformation pattern with the greatest deformation at the center of the basin.

Since Gilbert's first observations of this phenomenon, multiple studies have been carried out to characterize and quantify the rebound of the basin following removal of the lake. Adams and Bills (2016) utilized shoreline elevations measured by Currey (1982) at various locations across the basin to create palinspastically restored digital elevation

models (DEMs) for the Bonneville and Provo highstands. Rebound contours for the Bonneville and Provo levels are illustrated in Figure 4. The products of the Adams and Bills (2016) investigation are utilized in this study to discern between the isostatic and tectonic signals recorded by the Bonneville and Provo shorelines.

The Wasatch Fault Zone

Tectonic setting. The Wasatch Fault Zone is a 370 km segmented normal fault comprising the eastern border of the extensional Basin and Range Province. The classic segmentation model of the WFZ divides it into 10 independent segments, based primarily on structural complexities and bedrock salients (Schwartz and Coppersmith, 1984; Wheeler and Krystinik, 1992). The most seismically active of these are the five central segments: the Brigham City, Weber, Salt Lake City, Provo, and Nephi segments (Figure 5). While no historic surface-rupturing earthquakes have been recorded on these segments, paleoseismic trenching studies have identified 20 surface-rupturing earthquake events estimated to be greater than ~M 7.0 in the last 7 ky (DuRoss *et al.*, 2016).

Characterization of Brigham City and Weber segments. The Brigham City segment is the northernmost of the central segments, characterized by a 60° bend in the fault at Box Elder canyon that was defined as a subsegment boundary by Personius (1990). The primary linear length of the segment is 35 km, where the northern subsegment is 18 km and the southern subsegment is 17 km in length (DuRoss *et al.*, 2016). There have been four Holocene earthquake events on this segment based on paleoseismic trenching studies (Personius *et al.*, 2012; DuRoss *et al.*, 2016). A comparison of slip rates from the southern subsegment and northern subsegment reveals

significantly more events on the southern subsegment (Personius *et al.*, 2012). Personius *et al.* (2012) suggest that the southern subsegment of the Brigham City segment has experienced spillover rupture from the Weber segment, and that ruptures may be more likely to nucleate on the southern subsegment of the fault.

The Weber segment is the only one of the central segments without a subsegment boundary or significant structural complexities (DuRoss *et al.*, 2016). It is also the longest of the central segments, with a primary linear length of 56 km. The continuous length of this segment merits it as a significant seismic hazard, capable of producing earthquakes M 7.0-7.2 (DuRoss, 2008). Five Holocene events have been identified on the Weber segment, as well as the potential for partial segment ruptures (DuRoss *et al.*, 2016).

Brigham City – Weber Segment boundary. The Brigham City – Weber segment boundary is characterized by the Pleasant View Salient, a complexly faulted bedrock salient with significantly decreased throw, or vertical component of slip (Figure 6). It is unclear as to whether preexisting faults throughout the salient are reactivated by ruptures on the Brigham City and Weber segments (Personius *et. al*, 2012). At least one spillover rupture from the Weber to the Brigham City segment has been identified from Holocene trenching data (Personius *et al.*, 2012; DuRoss *et al.*, 2016). Increased Holocene displacement on the northern Weber Segment near the segment boundary is interpreted by DuRoss and others (2016) as evidence for mechanical interaction between the two segments.

Theoretical fault displacement models. Along-strike displacement for the individual segments of the WFZ has been modelled (Chang and Smith, 2002; DuRoss,

2008) using a half-ellipse displacement pattern for simple linear elastic fracture (Watterson, 1986; Watterson and Walsh, 1987). In this model, the displacement is greatest at the center of the fault and zero at the tips (Figure 7a). The half-ellipse model corresponds to faults or fault segments that rupture independently, where the zero displacement at the tips represents a complete stress drop caused by strong fault boundaries or strong segment boundaries (Ward, 1997).

Earthquake ruptures can also terminate in areas of low stress where energy is gradually dispersed. In this case, there is an incomplete stress drop that exhibits a concave-up displacement pattern at the termination of the rupture (Figure 7b), which can occur anywhere along the fault (Ward, 1997). Fault segments can also mechanically interact or link over time. Mechanically interacting faults at fault step-overs exhibit a shift in maximum displacement to the area of overlap between fault strands (Figure 7c) (Willemse *et al.*, 1996), while linked fault segments exhibit decreased displacement at the former segment boundary (Peacock and Sanderson, 1991; Figure 7d).

The half-ellipse model has been empirically validated for Basin and Range normal faults (Olig, 1994; Pezzopane and Dawson, 1996) and applied as a standard model for individual segments of the WFZ. Given the structural complexity of the WFZ, however, any combination of the described displacement models could manifest in the elevation profiles of Lake Bonneville shorelines.

Purpose

The WFZ poses a seismic risk to 80% of Utah's population, or approximately 2.3 million people. Current risk assessments are based primarily on:

1) Holocene vertical slip rates derived from paleoseismic trenching.
2) The classic fault segmentation model (Schwartz and Coppersmith, 1984; Wheeler and Krystinik, 1992).

The majority of seismic hazard analyses treat the segments of the WFZ as seismogenically independent segments that rupture along their full length (Wong *et al.*, 2016). Several paleoseismic studies suggest that partial and multisegment ruptures are possible (Chang and Smith, 2002; DuRoss, 2008; DuRoss *et al.*, 2016), which complicates our understanding of the fault system and the development of seismic risk assessments. DuRoss *et al.* (2016) establish the need for further investigation into the probabilities of these rupture scenarios. Holocene trenching data also indicate that some segment boundaries, considered barriers to rupture in seismic hazard analyses, are mature fault zones that can facilitate rupture. Classically defined segment boundaries also need to be investigated further to improve our understanding of the fault system.

Neotectonic analysis of Lake Bonneville shorelines is an alternative to trenching for understanding segment boundaries and further constraining seismic hazard analyses. Vertical slip rates measured from displaced Bonneville and Provo shorelines establish a Pleistocene perspective of the temporal and spatial pattern of surface ruptures, while kilometer-scale elevation profiles of measured shoreline paleoelevation serve as a geomorphic test for the generally accepted segmentation model. While the deformation of Lake Bonneville shorelines cannot provide insight to the rupture length of single events, it represents cumulative deformation since the late Pleistocene and can provide insight into the most probable rupture scenarios.

Scope

The scope of this study is limited to the Brigham City and Weber segments of the WFZ. Of the 5 central segments, only the Brigham City, Weber, and Salt Lake City segments contain shorelines with preservation sufficient to extract robust paleoelevation measurements. The Provo segment is the most heavily developed of the central segments, and anthropogenic activity has erased many shoreline features. Lake Bonneville at its highstand did not extend to the southern boundary of the Nephi segment, which makes this segment also unsuitable for analysis.

Neotectonic analysis of the Salt Lake City segment using Lake Bonneville shorelines was initially carried out by Jewell and Bruhn (2013), and we have chosen not to repeat their analysis using the PaleoElev tool in the scope of this study. In addition, the Brigham City and Weber segments contain the most abundant and well-preserved Bonneville and Provo shorelines. Therefore, these segments are the best choice for testing and applying the PaleoElev tool and neotectonic analysis of the WFZ.

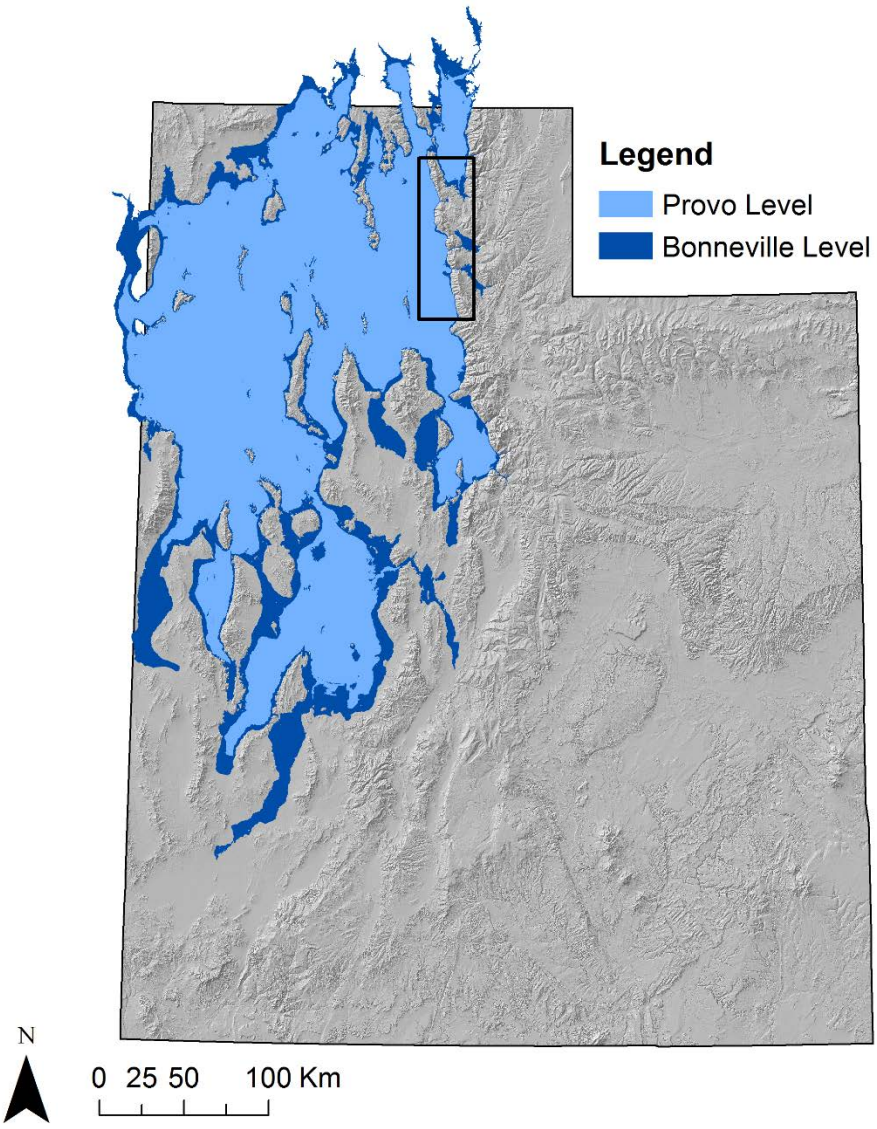

Figure 1. Isostatically corrected Bonneville and Provo highstands of Lake Bonneville. The black box represents the study area for this investigation. Lake shapefiles were provided by Ken Adams from data compiled in Adams and Bills (2016).

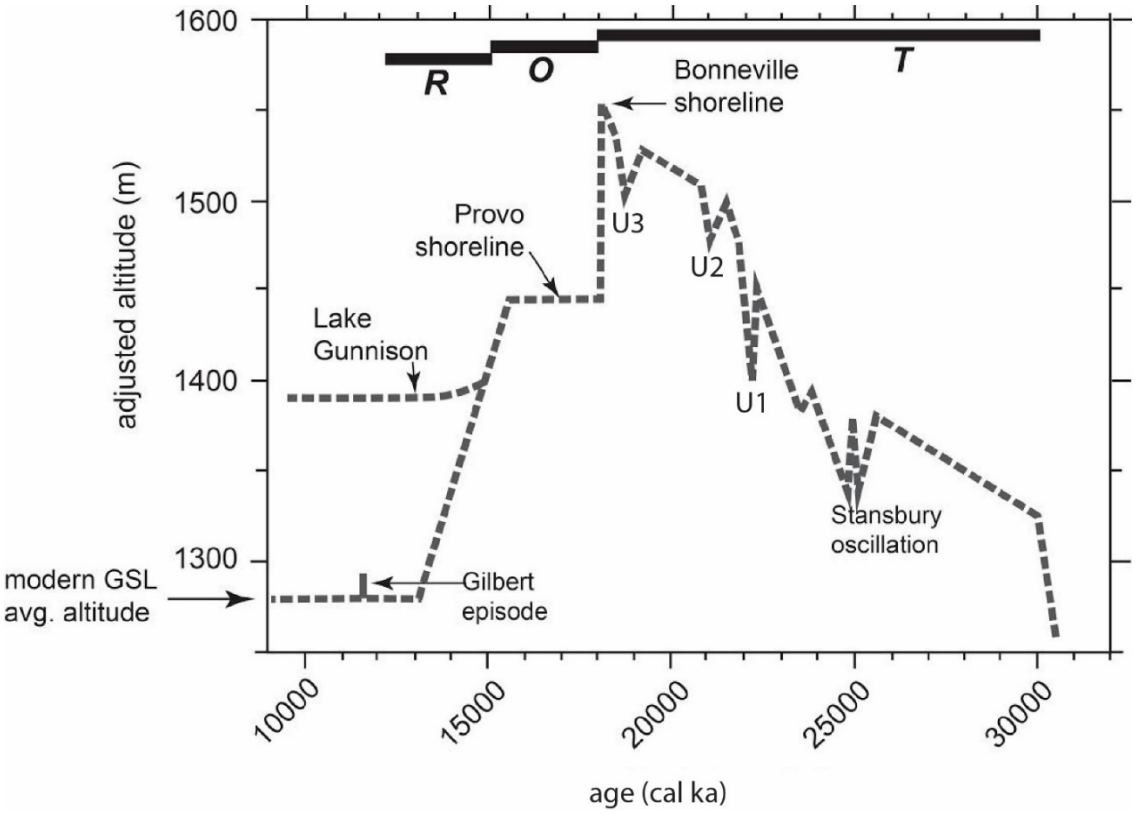

Figure 2. A Lake Bonneville hydrograph. R, O, and T correspond to the regressive, overflow, and transgressive stages of the lake's history. U1, U2, and U3 are unnamed oscillations. Figure reproduced from Charles G. Oviatt (personal communication, unpublished work).

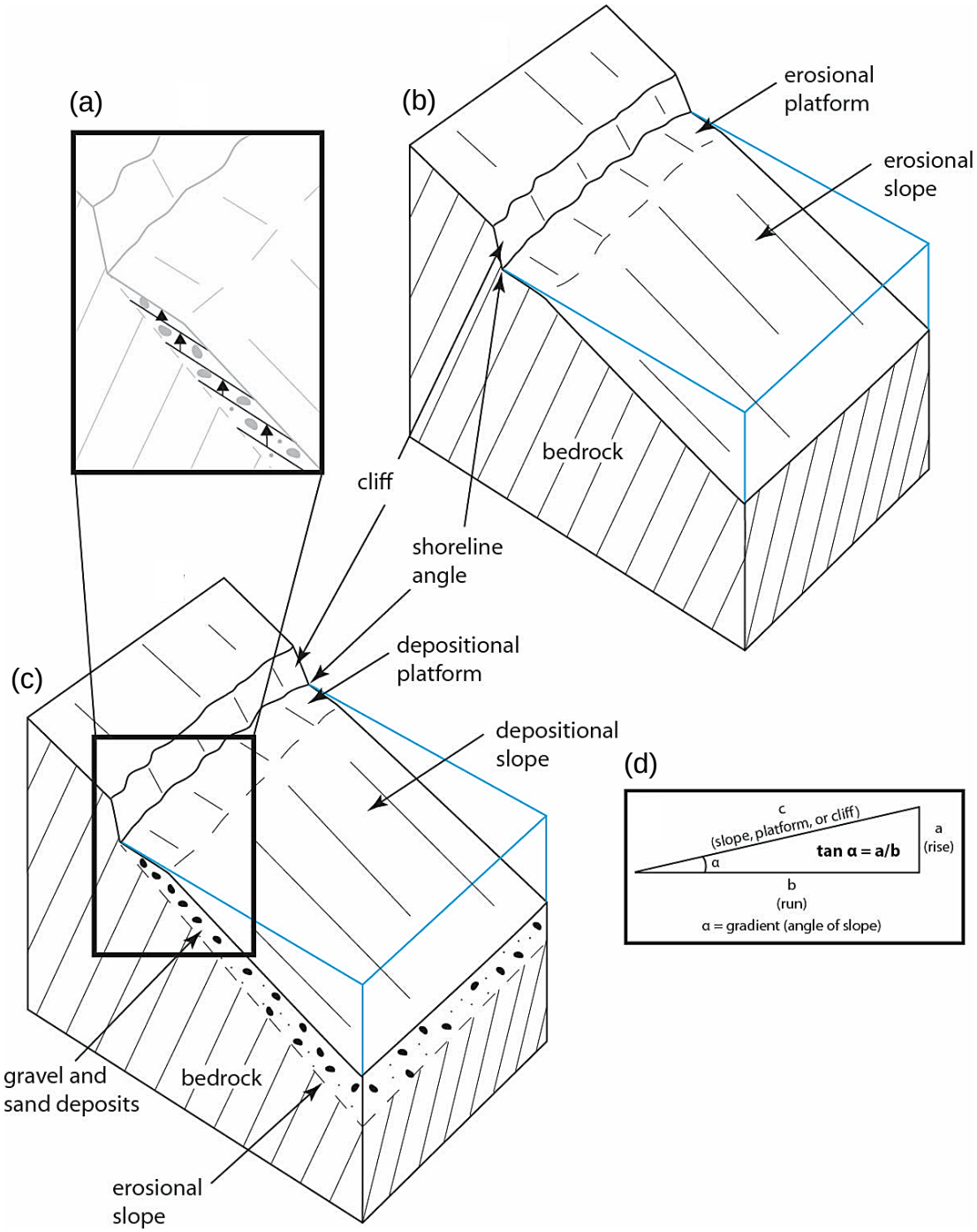

Figure 3. Shoreline morphology of depositional and erosional terraces. (a) Detail of deposits on a depositional terrace. (b) An erosional terrace, the expected morphology of the Provo shoreline. (c) A depositional terrace, representing morphology of the Bonneville shoreline. (d) A geometric example of shoreline slope. Figure reproduced from Oviatt and Jewell (2016).

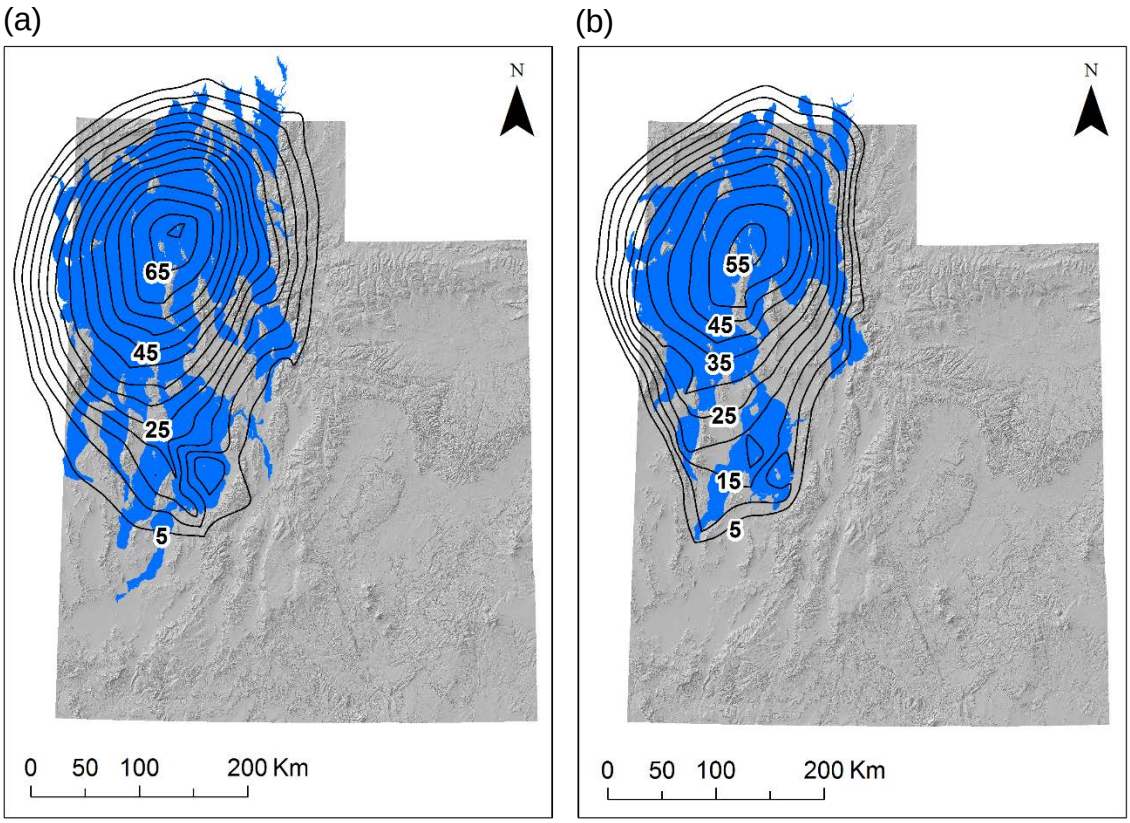

Figure 4. Isostatic rebound contours associated with the Bonneville and Provo highstands. The contour interval is 5 m. (a) Rebound contours for the Bonneville highstand, where the greatest rebound (center of the basin) is 73 m. (b) Rebound contours for the Provo highstand, where the greatest rebound (center of the basin) is 58 m. These contours were produced from 30 m DEMs of isostatic rebound provided by Ken Adams from data compiled in the Adams and Bills (2016) investigation.

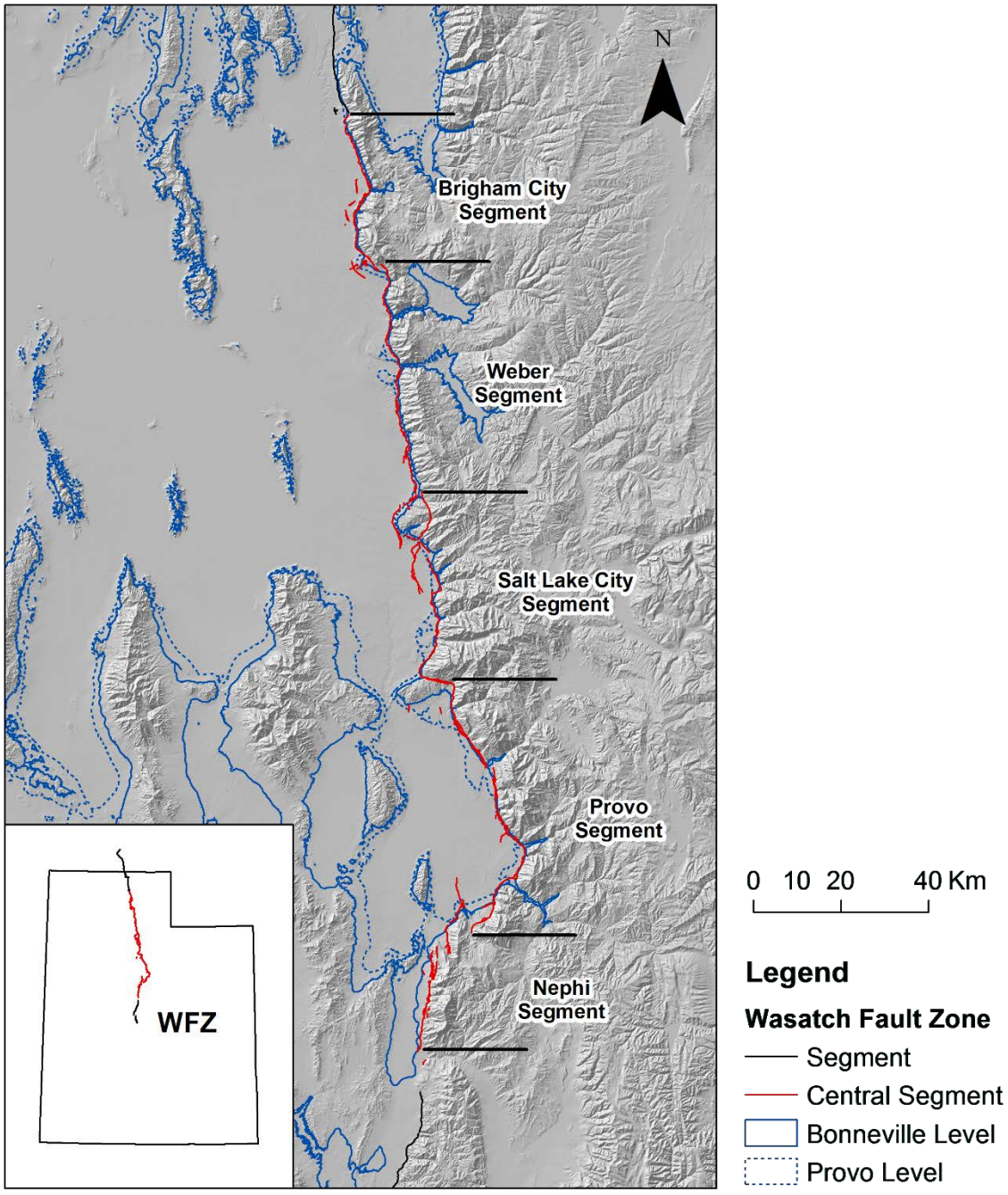

Figure 5. The central segments of the Wasatch Fault Zone.

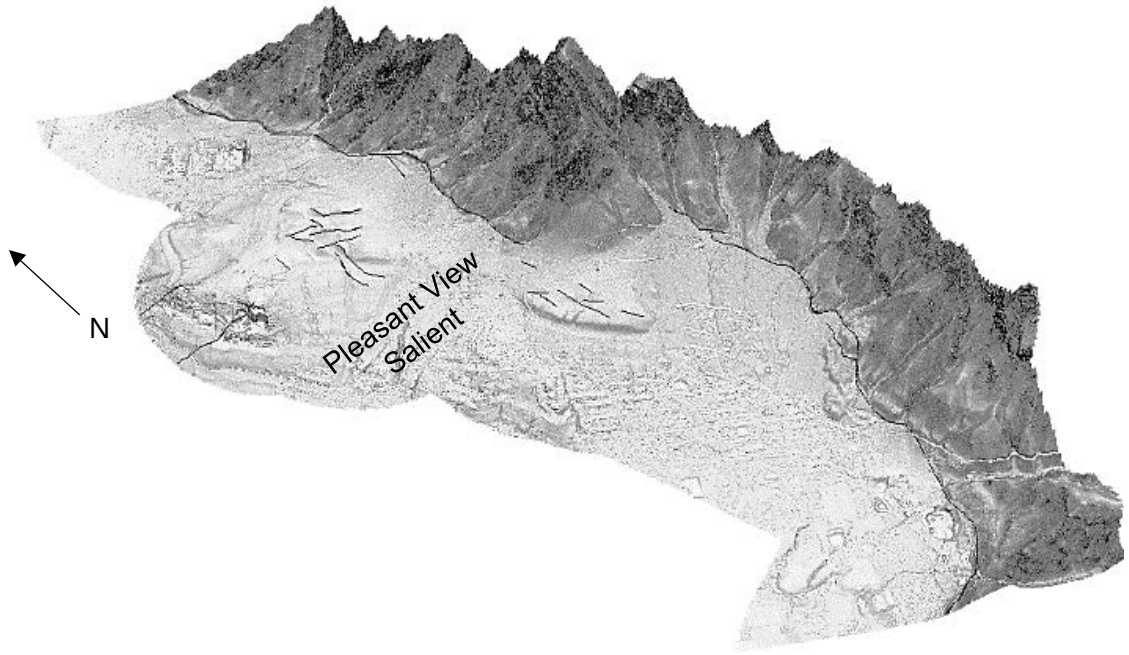

Figure 6. Brigham City – Weber segment boundary. The WFZ is shown here in black. The Brigham City segment is located to the north, terminating at the Pleasant View Salient. The Weber segment is located to the south.

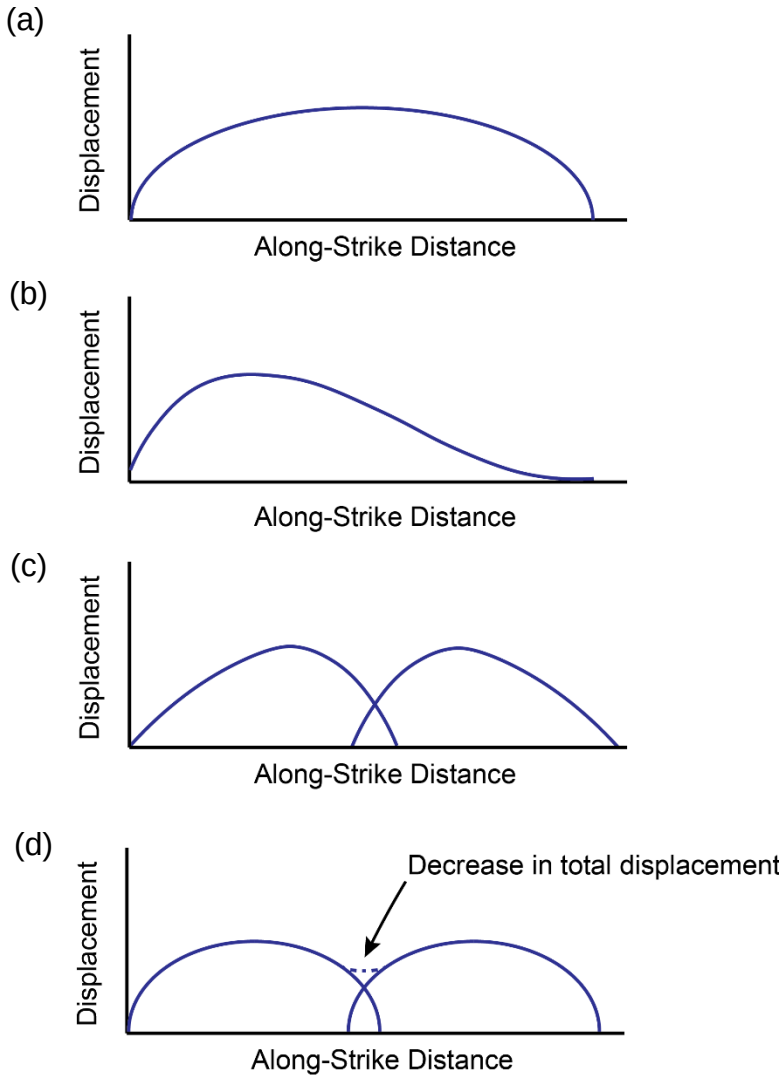

Figure 7. Theoretical models of along-strike fault displacement. (a) Half-ellipse displacement model based on simple linear fracture mechanics. Adapted from Watterson (1986) and Walsh and Watterson (1987). (b) Dogtail displacement model, where rupture gradually terminates in a low stress zone. Adapted from Ward (1997). (c) Displacement model for mechanically interacting faults in a fault step-over zone, where the maximum displacement occurs within the fault overlap. Adapted from Willemse *et al.* (1996). (d) Displacement model for linked fault segments, where the former segment boundary exhibits decreased displacement. Adapted from Peacock and Sanderson (1991).

MEASURING SHORELINE PALEOELEVATION

Theoretical Framework

Previous work. The shoreline angle, defined as the intersection between the wave-cut platform and wave-cut sea cliff (Kern, 1977), has long been considered the most robust geomorphic indicator of paleoelevation for shorelines and marine terraces (Bradley and Griggs, 1976). It should be noted that the shoreline angle is not truly reflective of an angle, but a point of intersection between two surfaces. Hereafter, the shoreline angle will be referred to as the shoreline datum. Pleistocene and Holocene shoreline features have experienced varying degrees of diffusion, burying the shoreline datum and complicating measurement of its elevation. Multiple methods have been developed to measure elevation of the shoreline datum beneath postformational colluvial wedges.

Meyer and Locke (1986) used qualitative criteria for surveyed shoreline profiles at Yellowstone Lake to project platform and cliff surfaces beneath colluvial wedges, where the intersection of the projections represents the location of the shoreline datum. Using a similar approach, McCalpin *et al.* (1992) projected platform and cliff surfaces based on criteria for the angle of the surface. Trenches excavated in this study showed these projections to be within 30 cm of what they identified as the top surface of Lake Utaho deposits, located in the Pocatello Valley at the border of Utah and Idaho (McCalpin *et al.*, 1992).

Expanding on these methods, Jewell and Bruhn (2013) applied quantitative criteria to constraining the platform and cliff in their analysis of Lake Bonneville shorelines. They used lidar DEMs to extract shoreline profiles and perform a second derivative analysis along each profile. Each shoreline platform and cliff were defined by inflection points along the shoreline profile and projected using linear regressions, where the intersection of the projections is the shoreline datum (Figure 8).

Measuring paleoelevation. This study expands on the Jewell and Bruhn (2013) approach to calculating paleoelevation. The second derivative of a shoreline profile is defined in this study as the second derivative parallel to slope, or profile curvature. Under this definition, negative values are convex, positive values are concave, and inflection points have a value of 0 (Figure 9). In an ideal model, the inflection point is analogous to a hinge across the shoreline surface where curvature equals 0. Inflection of a shoreline manifests not as a hinge, however, but as a zone where the shoreline surface is relatively planar (Figure 10). In this zone, the inflection point does not have an exact value of 0 but occurs where curvature changes sign.

Following the methodology of Jewell and Bruhn (2013), a linear regression through inflection points of both the shoreline platform and sea cliff are projected beneath colluvium on the shoreline bench (Figure 8). The intersection of these projections approximates the location of the shoreline datum, representing the best possible estimation of paleoelevation for a shoreline that has been modified by landscape diffusion. This method has proven to exhibit irregular results when shoreline morphology is affected by mass wasting, fluvial processes, or anthropogenic activity (Jewell and Bruhn, 2013).

Data Requirements and Description of PaleoElev Tool

The ArcGIS toolbox presented in this study was designed to automate calculations of paleoelevation. The methodology of Jewell and Bruhn (2013) employed manual data selection and analysis, which limited the resolution of data they were able to acquire to ~50-100 m on average. The PaleoElev tool efficiently measures paleoelevation with minimal manual inputs at a resolution specified by the user. The batch-processing capability of the tool also allows for analysis of swaths instead of single profiles. This modified approach incorporates the shoreline surface in its entirety, representing an averaging of the landscape in final paleoelevation calculations. Ultimately, the PaleoElev tool produces a more comprehensive dataset of paleoelevation than previous methods limited by the manual selection and analysis of profiles.

Development of PaleoElev as an ArcGIS toolbox allows for 100% of shoreline analysis to be carried out using ArcGIS software: there is no need to export lidar data to external software programs. The toolbox is composed of three scripts written in the Python programming language using the Python 2.7 integrated development environment (IDLE). These scripts utilize a combination of existing ArcGIS tools and custom Python functions developed as part of this study. Required extensions for the ArcGIS tools applied in PaleoElev include Spatial Analyst and 3D Analyst. Python modules required to operate these toolboxes include numpy (Python package for scientific computing), sympy (Python package for symbolic math), and math (Python package for mathematical functions). A simplified workflow for the toolbox is illustrated in Figure 11.

Inflection Points Script

Preprocessing input data. The required input data for the Inflection Points script are:

1) Polyline shapefile of mapped shorelines.
2) High-resolution DEM raster that covers the extent of the shoreline shapefile.

For best results, shorelines should be mapped as close as possible to the base of the sea cliff and exclude visible mass wasting, fluvial, or anthropogenic modifications (Figure 12). The input DEM must cover the full extent of the input shoreline polyline.

Description of Inflection Points Script. The purpose of this script is to create inflection points where a shoreline feature changes curvature. A workflow for this script is illustrated in Figure 13 and the required user-defined inputs and parameters are defined in Table 1. After input data and parameters are provided, the script creates swaths perpendicular to the mapped shoreline feature. To create the swaths, profiles are first generated using Mateus Ferreira's publicly available custom toolbox Transect2.0 (Cooley, 2014). This tool creates profiles perpendicular to the mapped shoreline at the length and spacing specified in the input parameters. Swaths are then created using the ArcGIS Buffer tool. This tool creates rectangles, at a width specified in the input parameters, around the profiles generated by the Transect2.0 toolbox. Once the swaths are created, the script performs the inflection point analysis for each swath in a loop.

The ArcGIS Focal Statistics tool is necessary to average swaths of the high-resolution input DEM (Figure 14a) in order to produce generalized curvature and inflection point outputs for each swath (Figure 14b, Figure 14c). Focal statistics performs an average for each cell in the DEM based on a user-defined neighborhood, which

includes a shape (rectangle, circle, or wedge, among others) and size. The script is set up so that if the neighborhood contains NoData values, which occurs at the edges of the swath, then all cells within the neighborhood are assigned values of NoData.

The assignment of NoData cells reduces low quality averaging at the edges of each swath, but also reduces the size of the swaths and produces edge effects (Figure 15). Both of these effects can be mitigated, however. Edge effects are removed based on user-defined parameter *m*, which reflects the maximum thickness of the edge effects. The maximum thickness of edge effects is dependent on the resolution of the input DEM. To mitigate size reduction, the user should specify a swath size larger than the desired swath size based on the size of the user-defined neighborhood in addition to the edge effect reduction parameter *m*.

After the swath has been processed using focal statistics, the curvature tool is used to produce a profile curvature raster. The final analysis in this script is the custom Python function Inflection_Function.py. This function requires input of the focal statistics raster, the profile curvature raster, and user-defined parameter *m*. Inflection_Function.py converts the input raster files to arrays, which establishes grids of curvature and elevation data across the xy extent of the swath. Grids for x and y values are produced from the minimum and maximum xy extents of the input curvature raster. Once these four grids are established, xyz coordinates can be indexed for inflection points in the curvature grid (Figure 16). To determine points of inflection, the curvature grid is analyzed row-by-row and column-by-column. An inflection point is indexed wherever the curvature changes sign (Figure 17).

Inflection_Function.py eliminates edge effects utilizing the user-defined

parameter *m*. The edge points of the input raster are identified and compared to calculated inflection points. Any inflection point that is within *m* distance of any edge point is excluded from the final output. After inflection results are filtered to exclude edge effects, the xyz coordinates are written to a multipoint feature class. The multipoint feature class for each swath is written to the final output, which is a multipoint feature class that holds all inflection points for the input shoreline feature (Figure 18).

Swath Profiles Script

The purpose of this intermediate script is to resolve the inflection points onto a profile in order to perform subsequent analysis in two dimensions. The required inputs for this script are both outputs from the Inflection Points script:

1. Inflection point multipoint feature class, produced by previous script.
2. Profile polyline, produced by previous script.

One user-defined parameter, a distance tolerance for points to be resolved onto a profile, must also be specified. In order to include all inflection points in the swath, it is recommended to use a tolerance larger than the swath size. In a loop, this script compares each swath of inflection points to its corresponding transect and uses the ArcGIS Snap tool to resolve the points onto the transect (Figure 19). The Swath Profiles script is only necessary for batch-processing. For a single profile, the ArcGIS Snap tool can be used directly to resolve inflection points onto a profile.

Shoreline Elevations Script

Preprocessing input data. To calculate paleoelevation, it is necessary to constrain calculated inflection points to the extents of the shoreline platform and sea cliff. These morphological features are naturally spatially variable due to post shoreline modification and the materials in which the shoreline formed. The extents of the shoreline platform and sea cliff must be mapped as individual polygons to constrain relevant inflection points (Figure 20). These shapefiles are required inputs for the Shoreline Elevations script. Extent polygons can be mapped using simply a hillshade or slopeshade of high-resolution DEMs, however, we recommend utilizing curvature rasters to aid in mapping these features.

Description of Shoreline Elevations Script. The purpose of the Shoreline Elevations script is to calculate paleoelevation using the inflection point data produced by the preceding scripts. This script requires input of the swath profiles produced from the Swath Profiles script and mapped extents of the platform and sea cliff. This script loops through the swath profiles and clips each profile to the input extents of the platform and sea cliff. If either of the clip outputs are empty, then the script continues to the next swath profile. If both clip output files contain points, then the custom function Shoreline_Elevation_Function.py is implemented.

The Shoreline Elevations script designates the inflection points located on the platform and sea cliff as the inputs to the function. The function then extracts the xyz coordinates of these points. To fit a linear regression to the platform and cliff surfaces, the function resolves the xyz points into 2D space. In 2D, the x-axis corresponds to distance along the swath profile, where the minimum platform point is assigned a value

of 0. The y-axis corresponds to elevation, or the z coordinate.

The function then requires a minimum of two points for each surface. If this requirement is met, then the inflection points on each surface are fit with a linear regression, where the intersection of these projections is the paleoelevation (Figure 21). After this point is calculated, it is resolved back into xyz space using trigonometric principles of similar triangles (Figure 22). The function is equipped to handle any transect orientation. An example output of this function is illustrated in Figure 23.

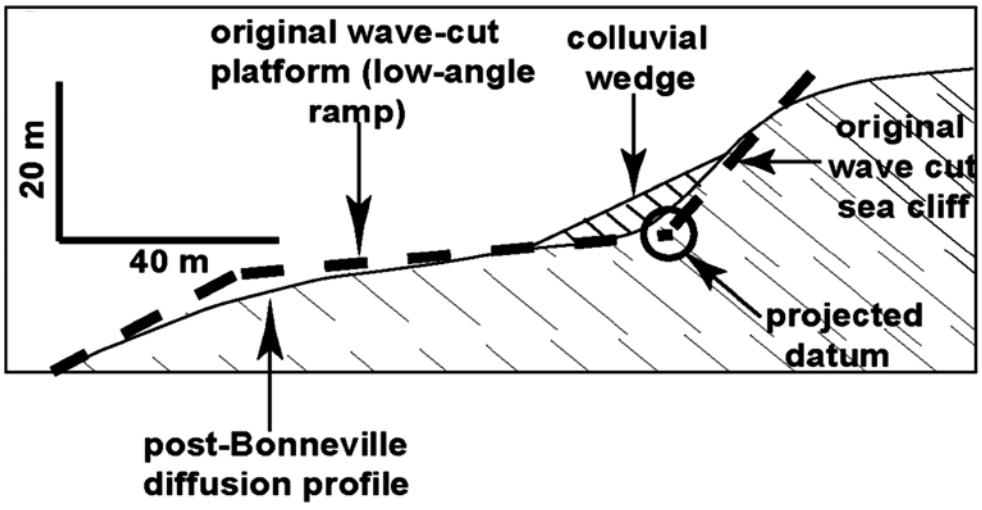

Figure 8. Generalized profile of a Lake Bonneville shoreline. The projected datum is the location of the original shoreline angle. Figure reproduced from Jewell and Bruhn (2013).

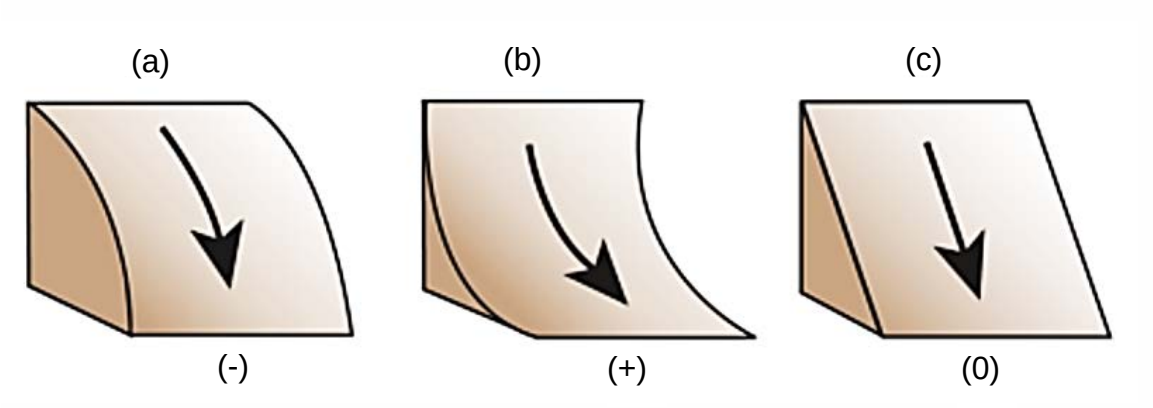

Figure 9. Schematic illustrating profile curvature. (a) Negative curvature (-) representing a convex surface. (b) Positive curvature (+) representing a concave surface. (c) A planar surface with 0 curvature. Modified from Environmental Systems Research Institute, Inc. (ESRI) ArcGIS Desktop Documentation (ESRI, 2016).

(a)

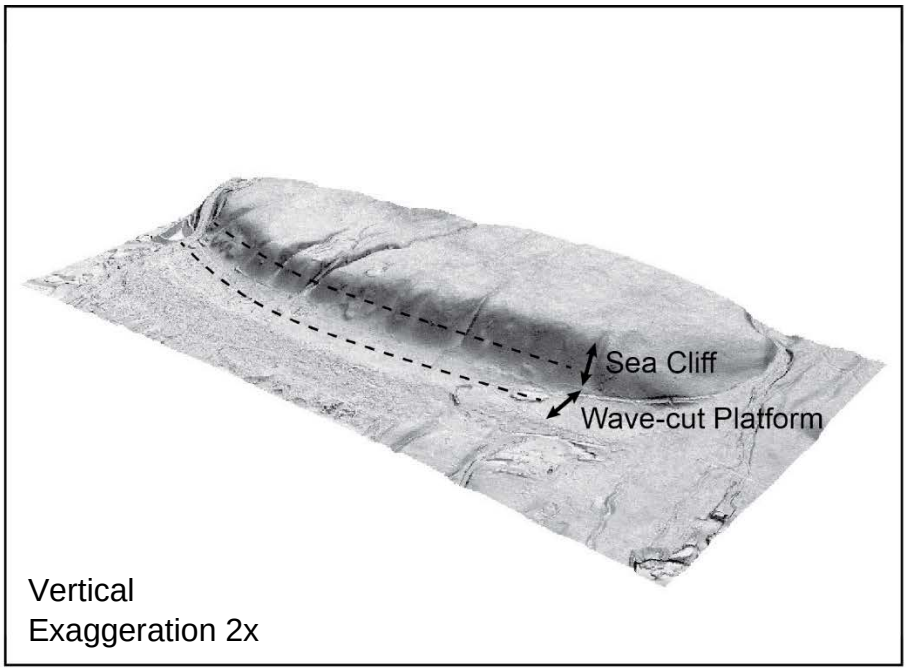

(b)

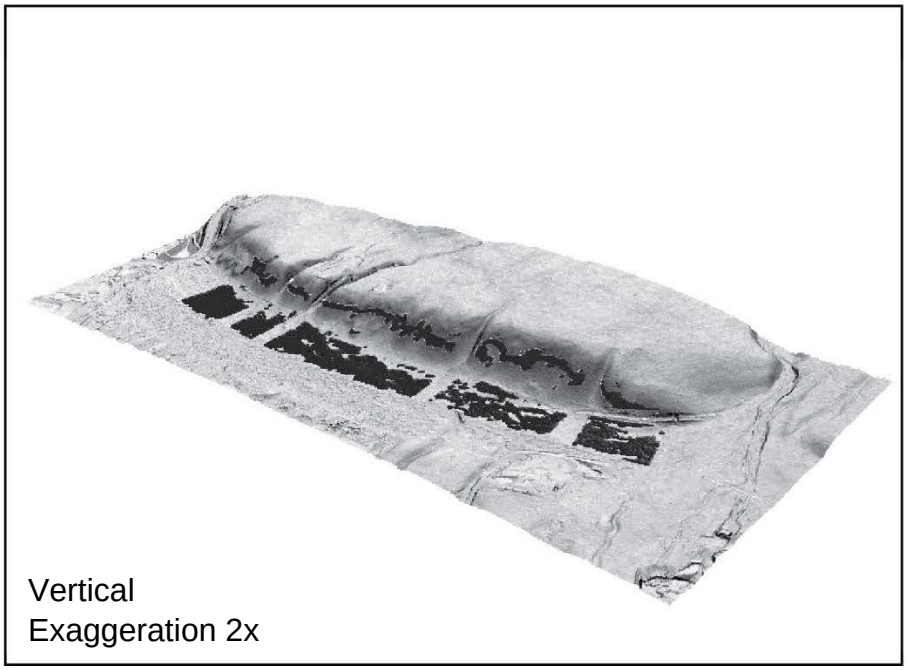

Figure 10. Inflection of a Bonneville shoreline. The shoreline in this example has been vertically exaggerated by a factor of 2. (a) Ideal inflection points shown as dashed lines for the shoreline platform and cliff. Arrows indicate the extents of the platform and cliff. (b) Calculated inflection points, excluding drainages, for the shoreline platform and cliff. Inflection points are shown in black. Base map is a slopeshade of 0.5 m lidar.

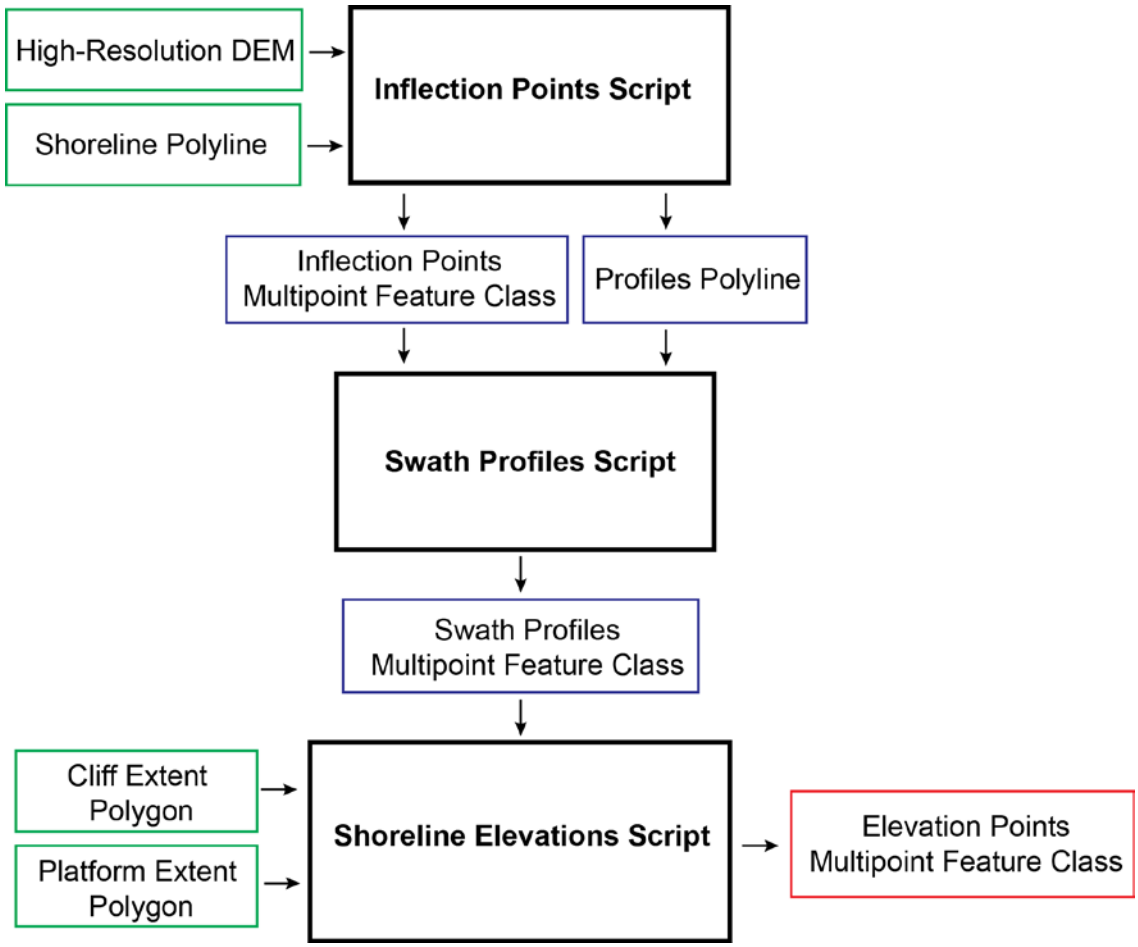

Figure 11. Generalized workflow for the PaleoElev toolbox. Black boxes represent the scripts in the PaleoElev toolbox. Green boxes are external inputs, blue boxes are intermediate outputs used as inputs to the subsequent scripts, and the red box represent the final output of the toolbox.

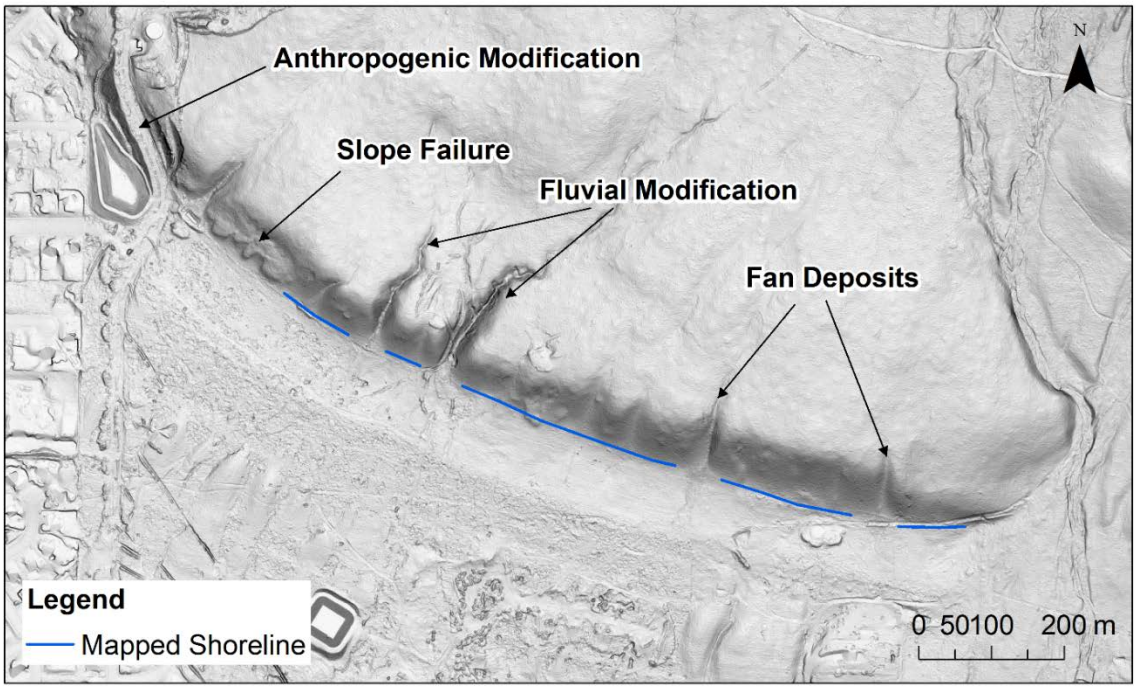

Figure 12. Example of a mapped shoreline. Note that the mapped shoreline excludes areas with visible modifications in addition to erosion. Base map is a slopeshade of 0.5 m lidar.

Table 1. Input data and parameters required by PaleoElev

1. Inflection Points Script		
Input Data	Data Type	Description
Output Folder	Workspace	Folder where output file will be saved
Mapped Feature	Feature Layer	Mapped geomorphic features
DEM	Raster Layer	Lidar or other high-resolution DEM
Transect2.0	Toolbox	Transect2.0 toolbox
Output File	String	Name of the output file
Parameters	Data Type	Description
Profile Spacing	Double	Integer of profile spacing. This value reflects the final resolution of paleoelevation points
Profile Length	Double	Integer of profile length. This value reflects half of the total length
Units	String	Units of profile length
Swath Width	Linear Unit	Requires value and units. This value reflects half of the total width
Statistics Neighborhood	Neighborhood	Recommended: NbrRectangle({width}, {height}, {units})
Maximum Thickness of Edge Effects	Double	Integer representative of the maximum width of edge effects

Table 1. Continued.

2. Swath Profiles Script		
Input Data	Data Type	Description
Output Folder	Workspace	Folder where output file will be saved
Profiles	Feature Layer	Output polyline feature class from the previous script
Inflection Points	Feature Layer	Output multipoint feature class from the previous script
Parameters	Data Type	Description
Swath Area	Linear Unit	Requires a value and units - recommended to use a value larger than the swath area
3. Shoreline Elevations Script		
Input Data	Data Type	Description
Output Folder	Workspace	Folder where output file will be saved
Swath Profiles	Feature Layer	The output file from the previous script
Cliff Extent	Feature Layer	Polygon shapefile of mapped cliff extents
Platform Extent	Feature Layer	Polygon shapefile of mapped platform extents

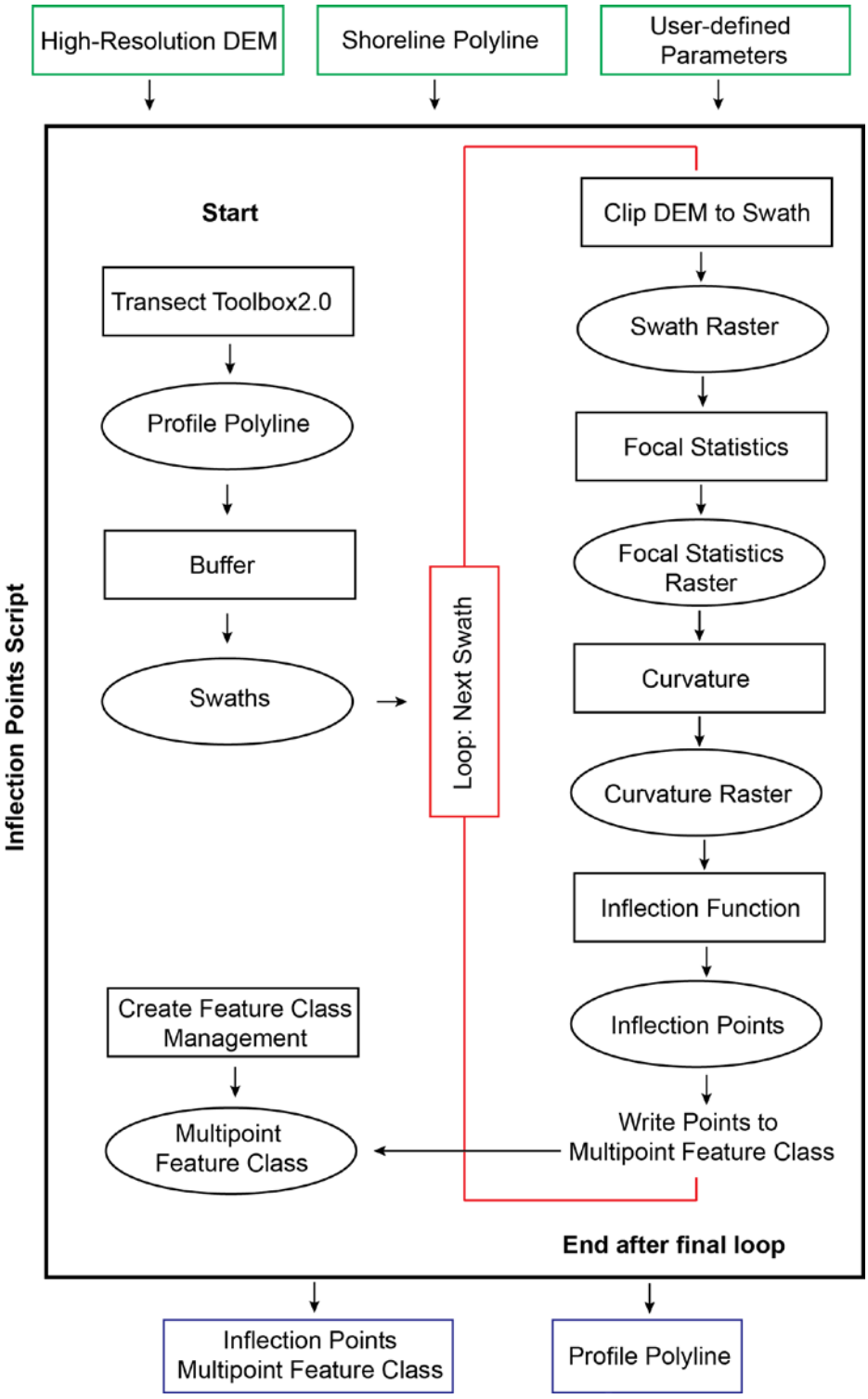

Figure 13. Generalized workflow of the Inflection Points script. Green boxes indicate required inputs and blue boxes are outputs. Black boxes represent ArcGIS and custom tools implemented in the Inflection Points script. Black ellipses are intermediate outputs utilized within the script.

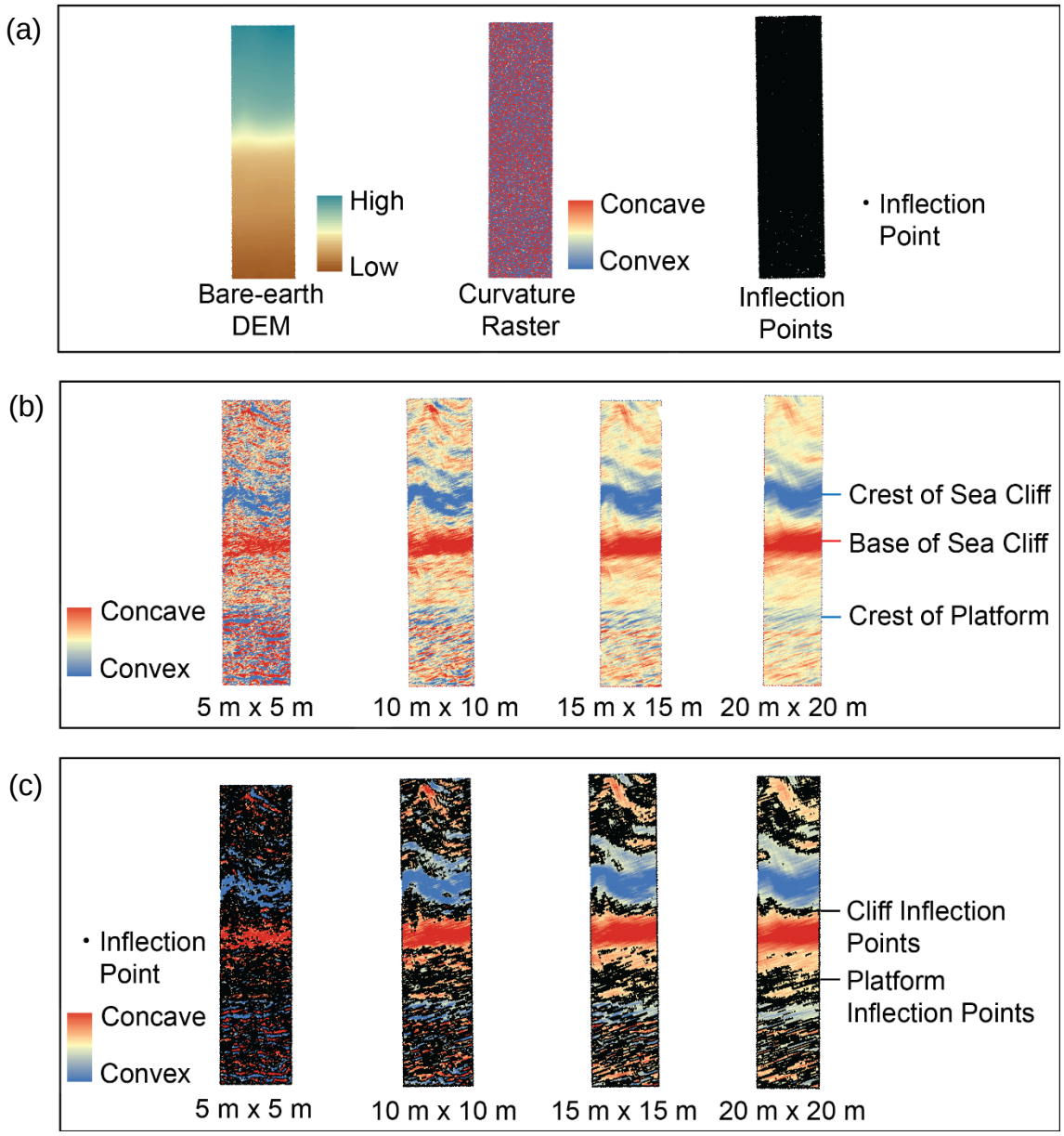

Figure 14. Example effects of mean focal statistics on curvature and inflection point output for a single swath. (a) Analysis of a lidar bare-earth DEM swath without application of focal statistics. (b) Curvature swaths with focal statistics applied. The size of the rectangular neighborhood is indicated beneath each swath. (c) Inflection points overlain on curvature swaths with focal statistics applied. The size of the rectangular neighborhood is indicated beneath each swath. Edge effects have not been removed in this example. Note that inflection points are created around the edge of each swath because of edge effects.

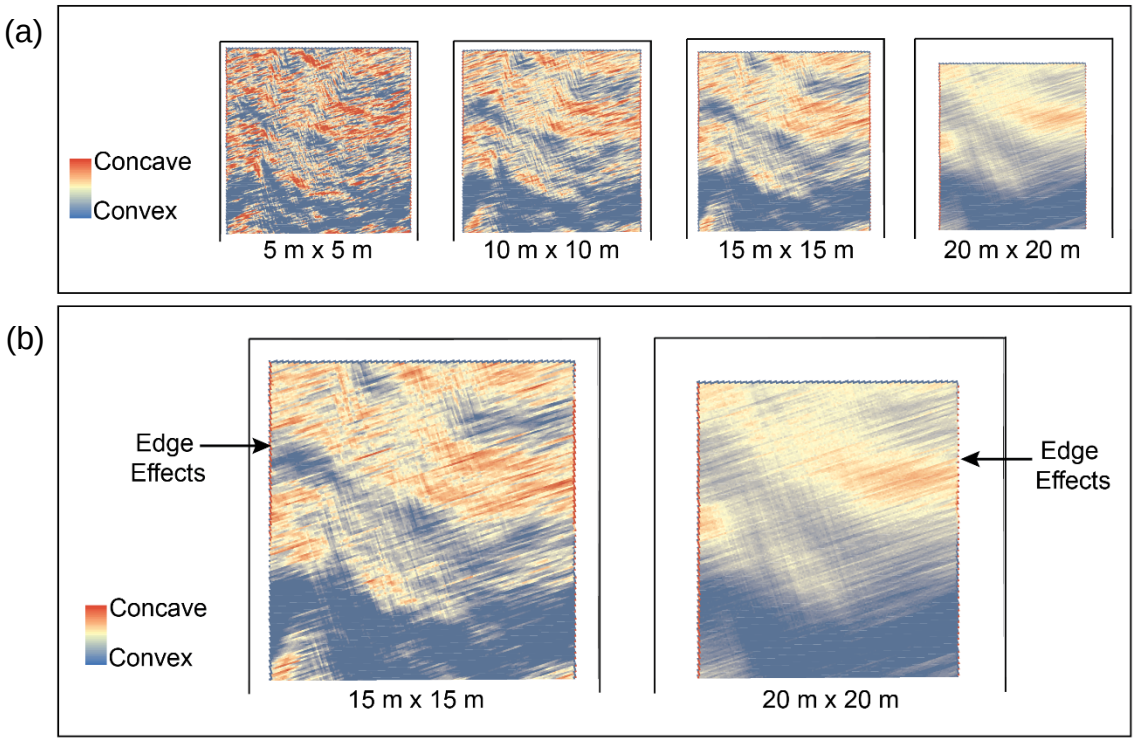

Figure 15. Size reduction and edge effects produced by mean focal statistics. The black border represents the original swath extent. (a) Magnitude of size reduction for different rectangular neighborhood sizes, indicated below each swath. (b) Edge effects for two swaths with different rectangular neighborhood sizes. The maximum thickness of the edge effects is constant regardless of neighborhood size.

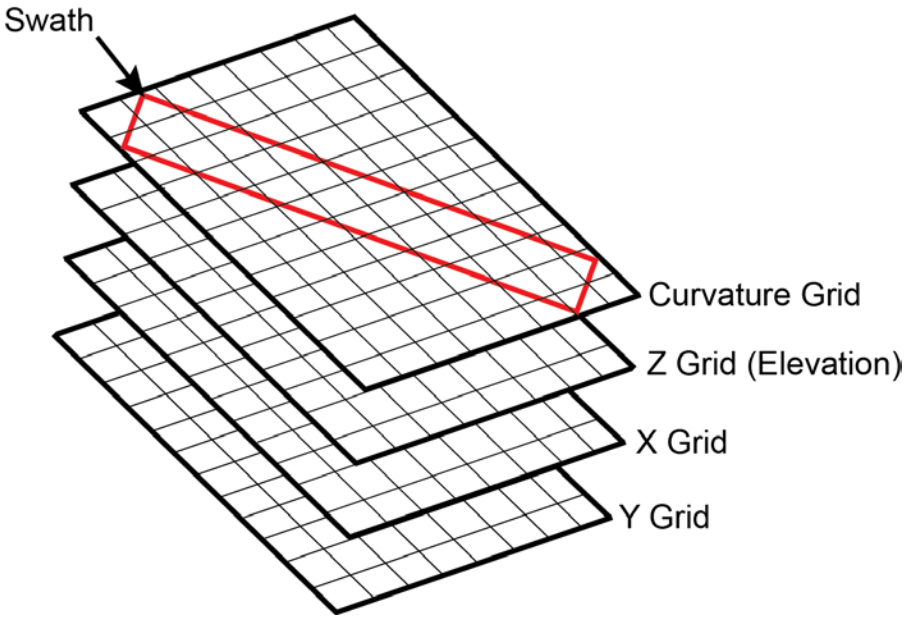

Figure 16. Schematic of grids created for each swath. The swath area is shown in red.

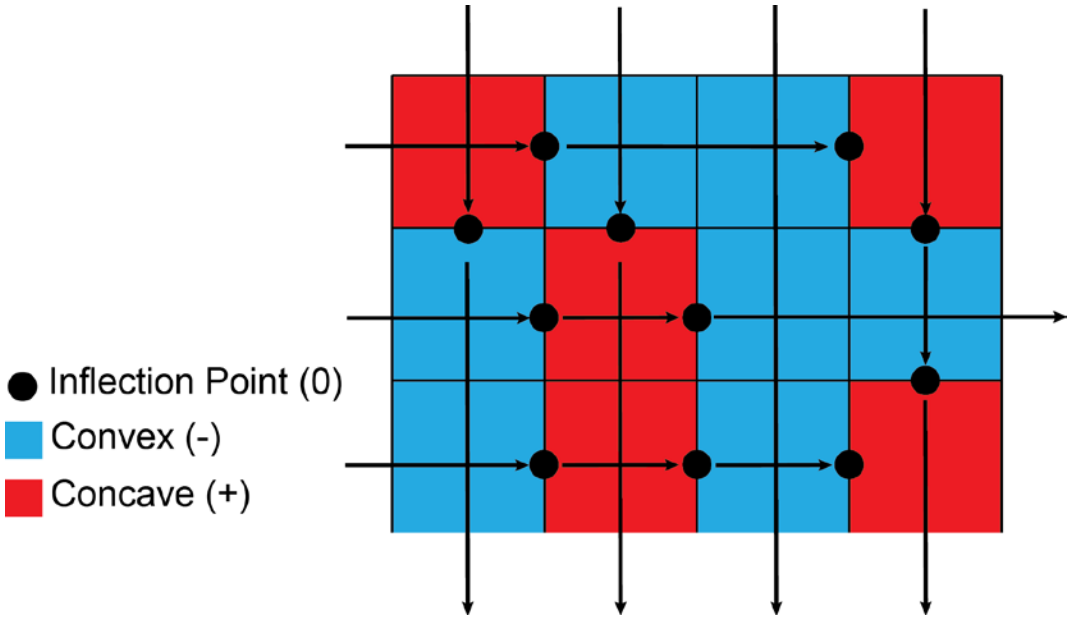

Figure 17. Schematic of inflection function producing inflection points. Vertical arrows represent column-by-column analysis and horizontal arrows represent row-by-row analysis.

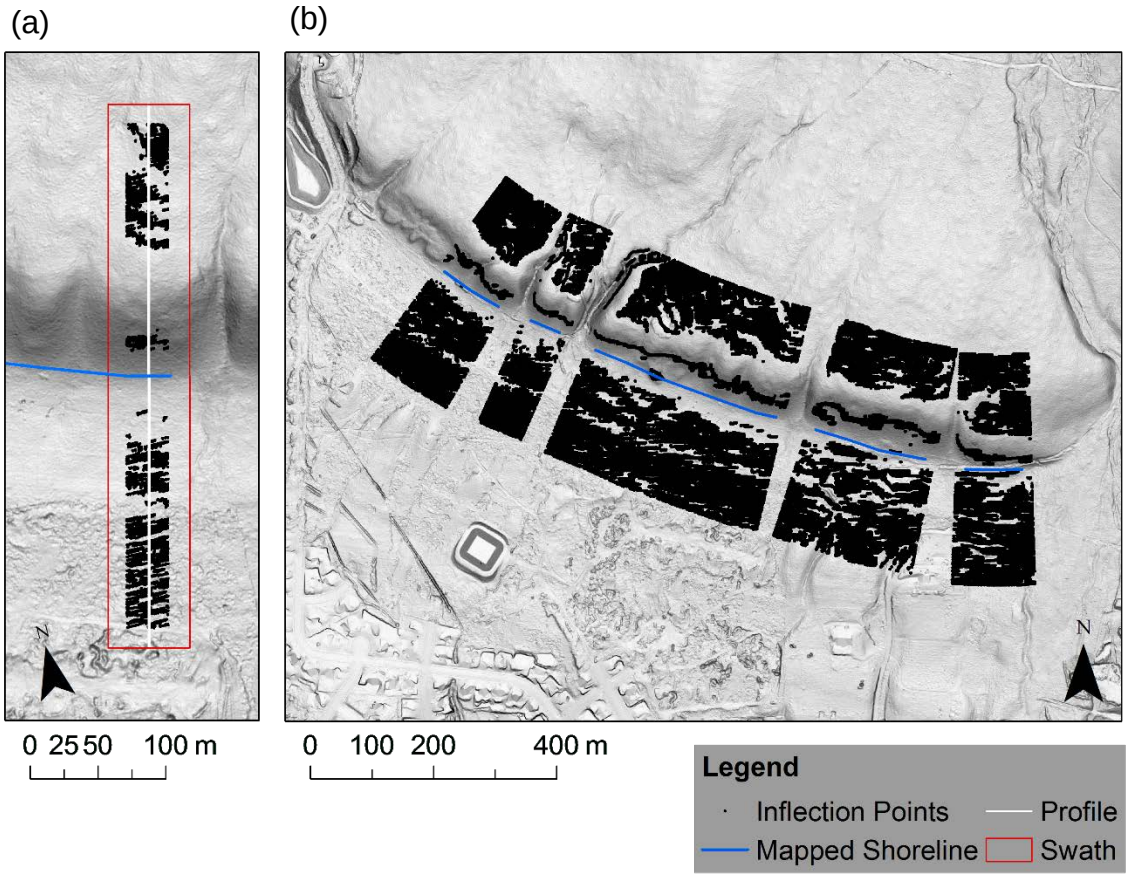

Figure 18. Example output of Inflection Points Script. (a) Output inflection points for a single swath. (b) Output inflection points for an entire shoreline feature. Base map is a slopeshade of 0.5 m lidar.

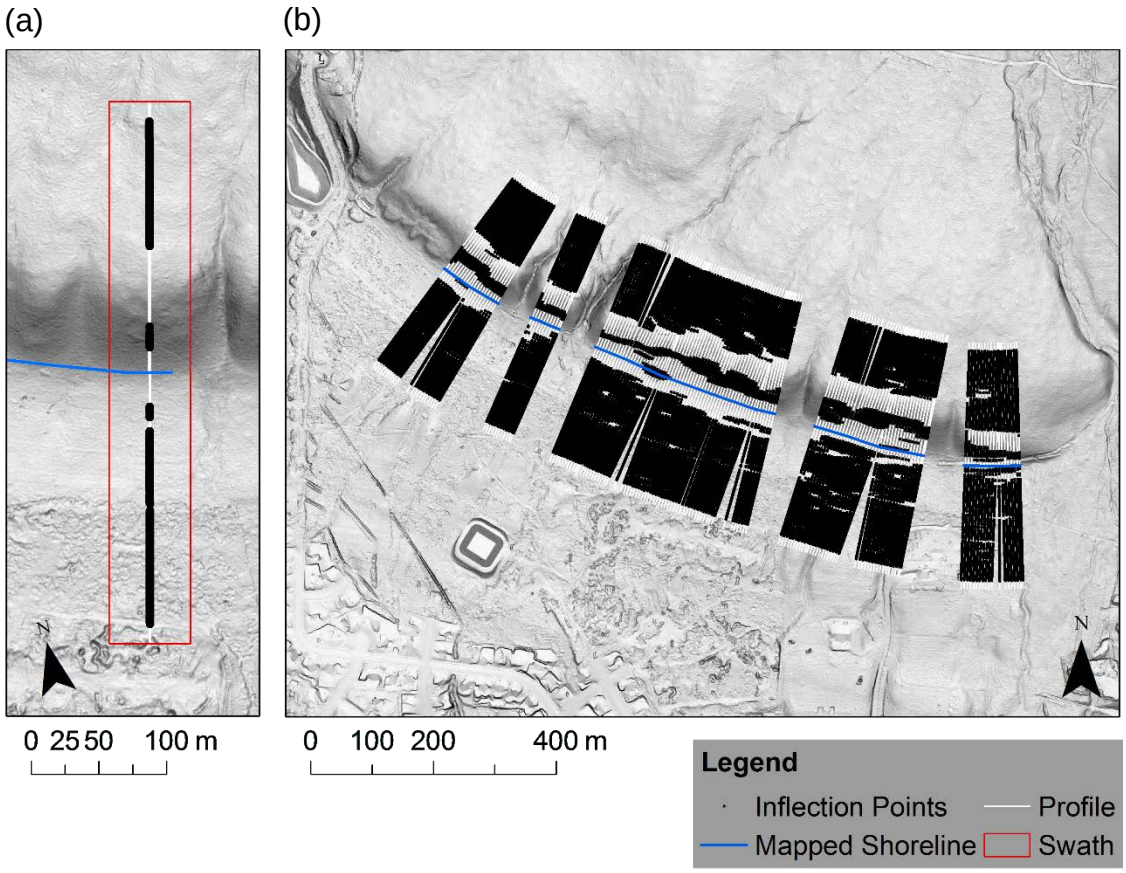

Figure 19. Example output of Swath Profiles Script. (a) Output for a single swath. (b) Output for an entire shoreline feature. Base map is a slopeshade of 0.5 m lidar.

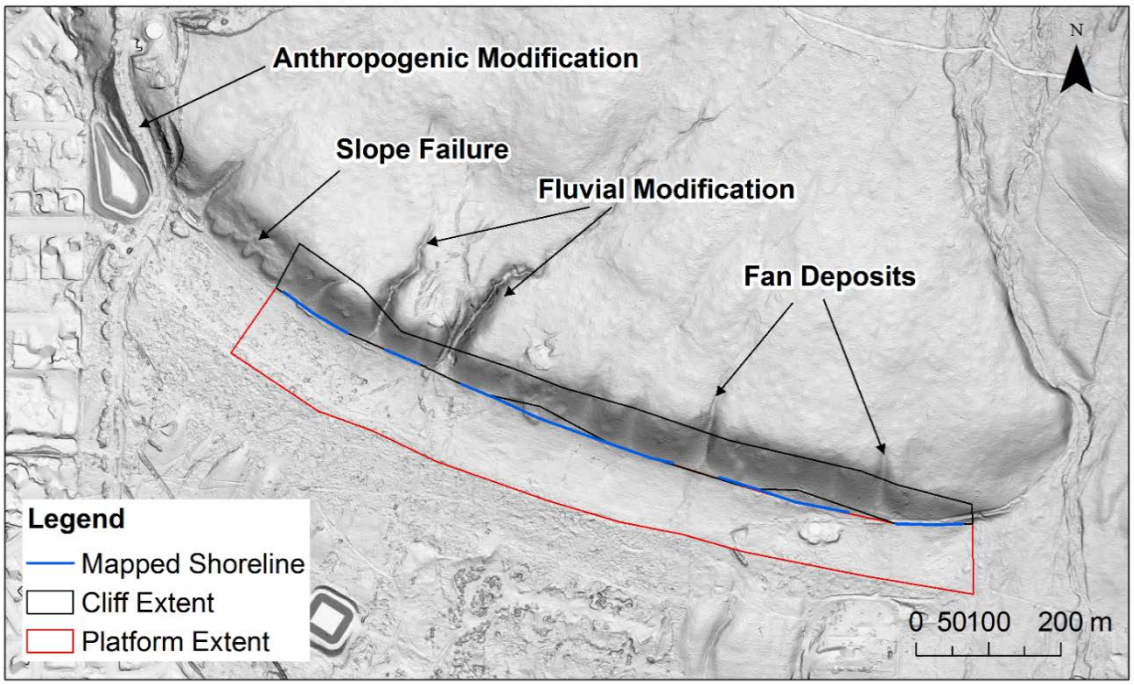

Figure 20. Mapped cliff and platform extents for a Bonneville shoreline. Base map is a slopeshade of 0.5 m lidar.

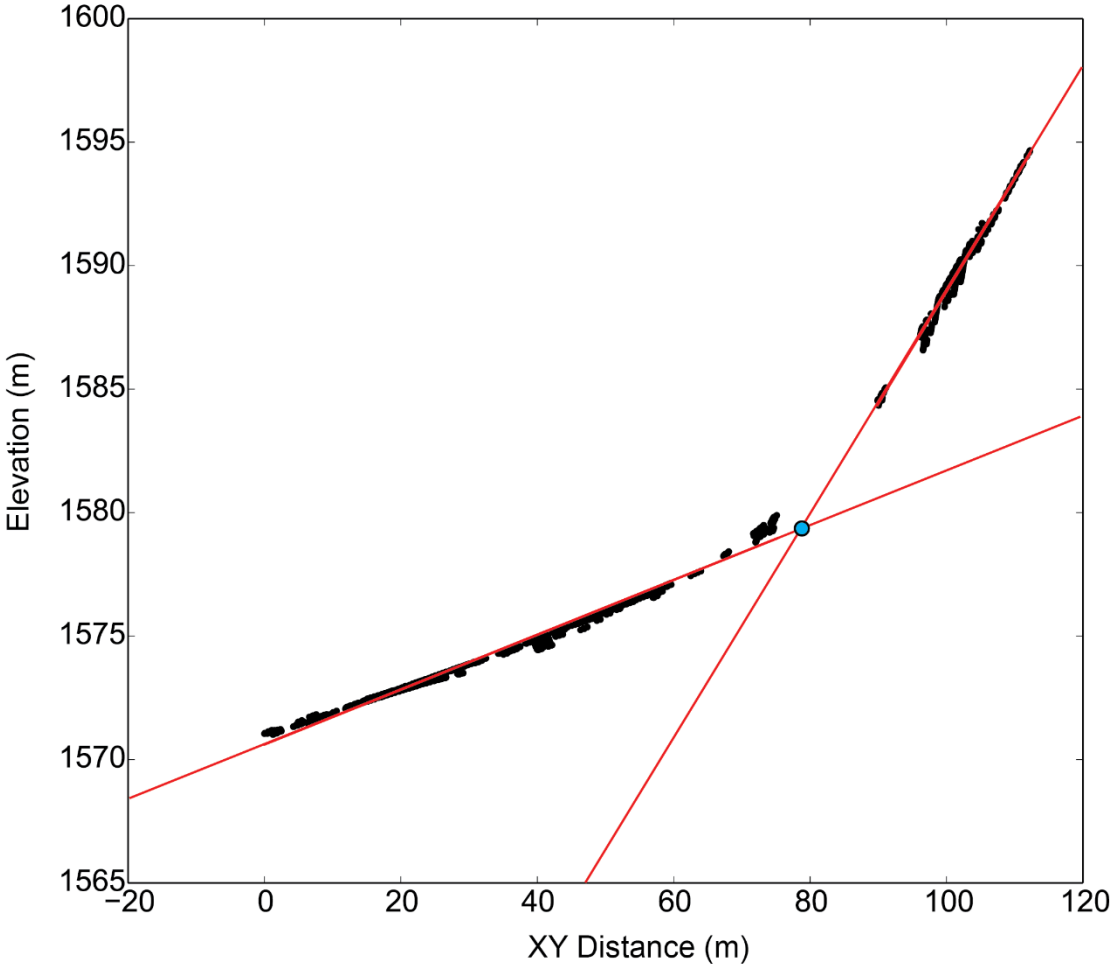

Figure 21. Example projection of a Bonneville shoreline paleoelevation datum point. Black points represent inflection points along the swath profile. Red lines represent linear regressions, where their intersection is the paleoelevation datum point calculated by the function. The paleoelevation datum point is shown in blue, and enlarged for clarity.

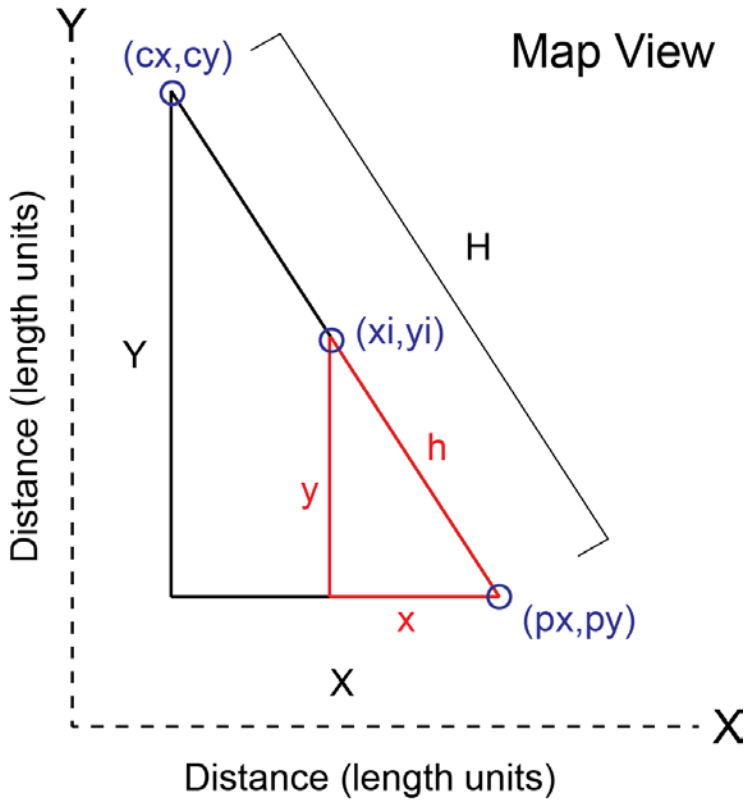

Figure 22. Trigonometric relationship used to resolve inflection point to xy space. X, Y, H, x, y, and h are all calculated distances from the 2D projection of the elevation point (xi, yi). Points (px, py) and (cx, cy) represent the minimum platform point and maximum cliff point, respectively. The calculated distances are added or subtracted from the xy coordinates of the platform (px, py), depending on the orientation of the profile, to determine the xy coordinates of point (xi, yi).

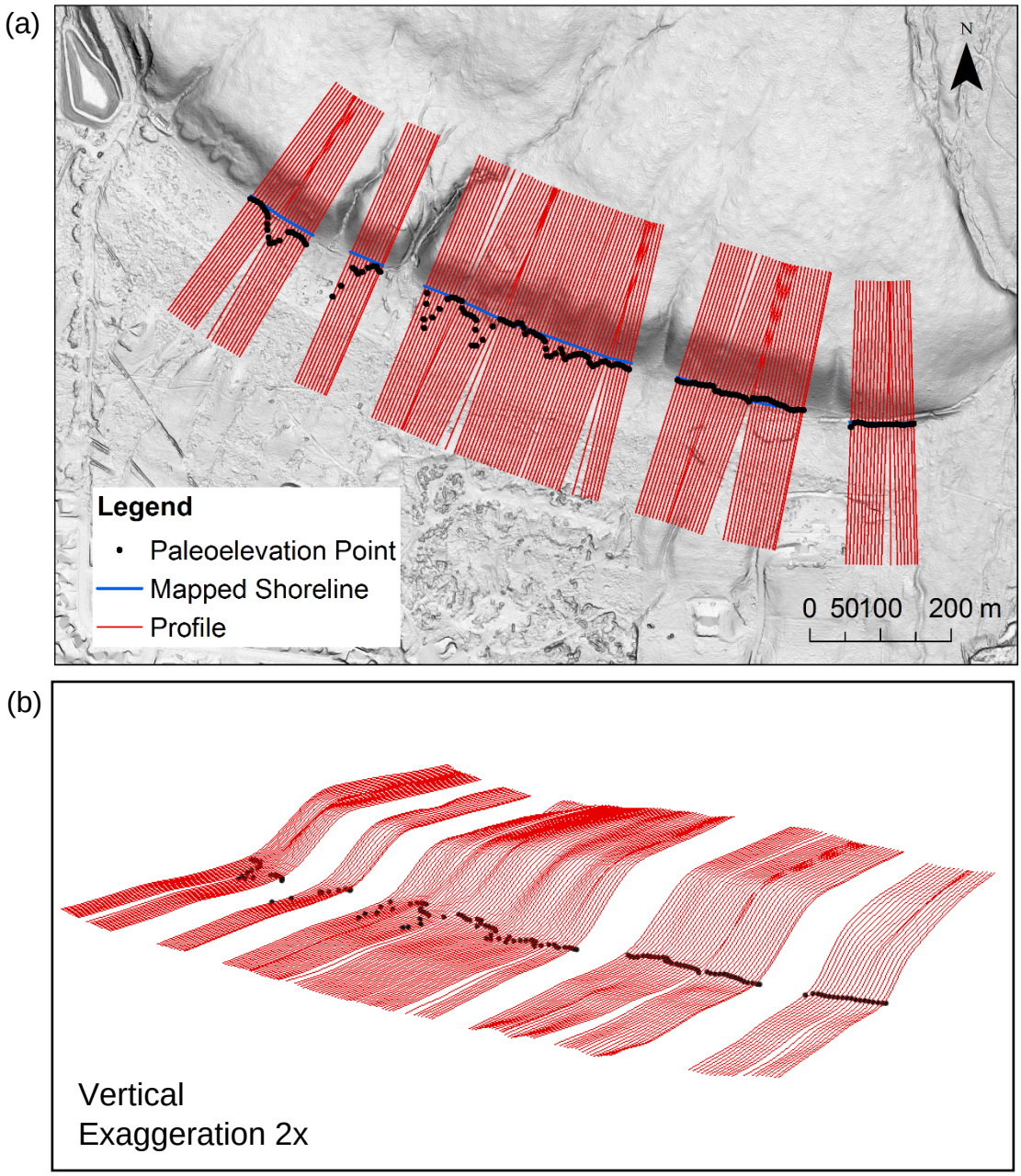

Figure 23. Example output of the Shoreline Elevations Script. (a) Map view of elevation points produced by the script. Base map is a slopeshade of 0.5 m lidar. (b) 3D view of shoreline elevation points.

APPLICATION OF PALEOELEV TOOL TO LAKE BONNEVILLE SHORELINES

Analysis of Bonneville and Provo Shorelines

Assumptions and inputs to PaleoElev. To apply the PaleoElev tool to Lake Bonneville shorelines we make the following assumptions:

1) Shorelines were approximately the same elevation at the time of formation.
2) Diffusion of the sea cliff has been the primary source of sediment for the colluvial wedges on the shoreline platforms.

Mapped shorelines represent the most well-preserved shorelines along the Brigham City and Weber segments (Figure 24). Poorly preserved Bonneville and Provo shorelines are identifiable in the lidar data, but were not mapped for purposes of this analysis. Publicly available bare-earth DEMs of 0.5 m lidar (http://gis.utah.gov/data) were used exclusively in measurement of paleoelevation for mapped shorelines.

The parameters chosen for analysis of Bonneville and Provo shorelines using the PaleoElev tool were based on observations and measurements of the shoreline features (Table 2). The input parameter profile length of 400 m and swath width of 60 m correspond to a swath size of ~370 m by ~30 m after mean focal statistics and removal of edge effects were applied. Small ~30 m swath widths are preferred over wider swaths because shorelines curve where they change strike in response to topography. Using a relatively small swath width ensures that a linear projection of inflection points in a swath

profile is a reasonable approximation of the land surface. Larger swath sizes, while potentially averaging out greater small-scale shoreline variability, may not be approximated well by a linear regression.

Mean focal statistics were performed using a 20 m by 20 m rectangular neighborhood, which corresponds to the least possible averaging required to produce a generalized inflection point output for 0.5 m lidar (Figure 14c). Edge effects generated from application of mean focal statistics exhibit a maximum thickness of 3 m in the 0.5 m lidar, so this thickness was used as the edge effects reduction parameter (Figure 15b). The final input parameter required was utilized in the Swath Profiles script. A swath area of 50 m was chosen as a conservative parameter to ensure all inflection points in each ~30 m wide swath were incorporated in their respective swath profile.

PaleoElev outputs. The number of paleoelevation datum points ultimately produced by the tool was 4,283 for the Bonneville shoreline (Figure 25), as compared to a potential 4,756 points based on the number of swath profiles. Fewer well-preserved Provo shorelines were mapped, which is reflected in the total 3,571 paleoelevation datum points (Figure 26) produced by the PaleoElev tool. This output is compared to a potential number of 4,400 for the Provo shoreline. The total output is less than the potential output because the custom function Shoreline_Elevation_Function.py within the PaleoElev tool requires a minimum of 2 inflection points on the platform and 2 inflection points on the sea cliff to perform linear regressions for these surfaces. Even so, the number of output points produced by the PaleoElev tool is an order of magnitude higher than any previous study employing manual analysis of profiles.

Elevation profiles of the PaleoElev outputs (Figures 27a-30a) exhibit visible

outliers. We identify two primary causes for these outliers. First, an R^2 parameter is not currently included in Shoreline_Elevation_Function.py, so outliers are produced from poor fits of platform and cliff surfaces with low density inflection points. Secondly, while manual mapping was as thorough as possible, it is evident from the PaleoElev output that some poorly preserved shorelines were included in the PaleoElev analysis. These outliers are removed in a series of corrections following primary analysis by the PaleoElev tool.

Corrections Applied to PaleoElev Output Points

Isostatic rebound correction. Lake Bonneville shorelines preserve a cumulative record of surface deformation since their formation, which includes isostatic rebound in addition to tectonic deformation. Isostatic rebound is particularly relevant to shoreline measurements in this study, as compared to the Jewell and Bruhn (2013) study, because rebound contours are oblique to shorelines along the Brigham City and Weber segments (Figure 25, Figure 26). When rebound contours are parallel to the shoreline features, as is the case for the Salt Lake City segment, the rebound signal is constant throughout shoreline elevation measurements and does not significantly affect tectonic interpretation.

To isolate the tectonic signal in the PaleoElev outputs, we corrected the output paleoelevations for isostatic rebound. To do this, we utilized 30 m DEMs of the magnitude of isostatic rebound for both the Bonneville and Provo lake levels. These DEMs were provided by Ken Adams, produced as part of work published in Adams and Bills (2016). The rebound magnitude DEMs were produced from the shoreline elevations surveyed by Currey (1982). Adams and Bills (2016) did not attempt to remove shoreline elevations from this dataset that Currey (1982) observed as having been affected by local

tectonic activity. The wavelength of tectonic deformation is small-scale in comparison to the isostatic signal recorded in a basin-wide dataset of shoreline elevation, however, and so the tectonic signal does not have a significant effect on the rebound magnitude DEMs. For this reason, we consider use of the rebound magnitude DEMs to be a reasonable approach to correcting isostatic rebound for shoreline elevations in this study.

To determine the magnitude of rebound at each paleoelevation datum point, the xy location of each point was interpolated from the corresponding rebound magnitude DEM. The magnitude of rebound was then subtracted from the calculated paleoelevation for that point to produce a rebound corrected paleoelevation datum (Figures 27b-30b).

Preprocessing for outlier removal. To remove outliers, we performed a two-pass filter on the rebound-corrected PaleoElev outputs. In order to preserve kilometer-scale tectonic trends, we performed these analyses on continuous shoreline sections (Figure 28, Figure 30). We define a continuous shoreline section as having no gaps in data greater than 300 m. Therefore, a shoreline is considered continuous if it is has small-scale discontinuities such as narrow drainages or fan deposits, but is not continuous across major rivers, areas of significant anthropogenic modification, or other factors contributing to large-scale discontinuities. Based on these criteria, we performed a two-pass filter to eliminate outliers on 52 continuous Bonneville shoreline sections and 37 continuous Provo shoreline sections.

Adjacent point filter. The first filter reduces point to point perturbations in elevation caused by poor projections from the code or small-scale surface variability caused by modification other than landscape diffusion (Figures 27c-30c). Acceptable points are defined as having an elevation difference of < 1 m from neighboring points, or

a slope less than 20% based on a minimum horizontal resolution of 5 m. We assume that a slope greater than 20% between elevation points at this resolution is unreasonable based on the assumption that the shoreline is approximately horizontal at small scales. Each point is compared to the neighboring points on either side of it, and only has to meet the difference criteria of < 1 m as compared to one of its neighbors to be retained in the dataset. Because this filter is designed to remove small-scale outliers, its effects are best observed for single continuous Bonneville and Provo shoreline sections (Figure 28c, Figure 30c).

The adjacent point filter eliminated 1,070 outliers from the Bonneville dataset and 691 outliers from the Provo dataset, reducing the total number of points to 3,213 for the Bonneville dataset and 2,880 for the Provo dataset.

Statistical filter. Following application of the adjacent point filter, the statistical filter is designed to eliminate outliers along each continuous shoreline section (Figures 27d-30d). These outliers are caused primarily by poor fits produced within the PaleoElev tool, so the effects of the statistical filter are best observed across the total paleoelevation dataset for the Bonneville and Provo shorelines (Figure 27d, Figure 29d).

First, we test whether the continuous shoreline sections exhibit a normal distribution. We calculate distance from the mean for each point in a shoreline section and compile these values for all continuous shoreline sections to produce a cumulative distribution. The distribution for each shoreline section is essentially stacked in the cumulative distribution, which gives greater weight to shoreline sections with higher point densities.

Both Bonneville and Provo continuous shoreline sections exhibit a normal

distribution, where the standard deviation for the Bonneville shoreline is ± 5.02 m and standard deviation for the Provo shoreline is ± 4.25 m (Figure 31). Outliers are eliminated in the statistical filter by restricting paleoelevation datum points to 3 sigma standard deviations from the mean of its respective shoreline section. The 3 sigma rule corresponds to 99.7% confidence bounds, so 99.7% of the dataset lies within the 3 sigma bounds.

The statistical filter reduces the number of points in the Bonneville dataset by 70 and reduces the number of points by 59 in the Provo dataset. As a result, the total number of paleoelevation datum points after application of the statistical filter is 3,143 for the Bonneville dataset and 2,821 for the Provo dataset.

Bonneville and Provo Shoreline Paleoelevation Measurements

Shoreline geomorphology. Once isostatic rebound is corrected and outliers are removed from the PaleoElev outputs, the remaining points in the Bonneville and Provo datasets are representative of robust paleoelevation shoreline datums (Figure 32, Figure 33). Any trends evidenced by these measurements are interpreted as real shoreline signals, not scatter produced as an artifact of the methods.

The total number of measurements in the Bonneville dataset is 3,143 and in the Provo dataset is 2,821. The standard deviation for each shoreline after all corrections have been applied is ± 4.89 m for the Bonneville and ± 3.99 m for the Provo. There is better coverage for the Bonneville shoreline along the Brigham City and Weber segments than the Provo shoreline, but Bonneville measurements are more variable. This difference can be attributed to difference in shoreline morphology, shoreline age, or greater

secondary modification of the Bonneville shoreline.

Relation to the Wasatch Fault Zone. In order to make neotectonic interpretations from shoreline paleoelevation, we classify shorelines by their location relative to the fault (Figure 32, Figure 33). Shorelines are classified as located on the footwall or hanging wall block of the main fault strand, where possible. The WFZ transitions from a single strand to a complex fault zone south of Brigham City, where some of the most well-preserved shorelines on the Brigham City segment are located. The fault strands within this zone cut across Bonneville and Provo shorelines, causing the shorelines to exhibit rapid elevation change over small distances (Figure 34, Figure 35). Sections of the Provo shoreline in particular have been noticeably down-dropped on hanging wall blocks within this fault zone (Figure 35). The Bonneville shoreline is more consistently located on the main footwall block within this fault zone, but is noticeably offset across a single non-parallel fault strand within the fault zone that cuts up Evans Canyon (Figure 34).

Interaction with the fault does not explain all of these elevation changes, however. The Bonneville shoreline just south of Box Elder Canyon, between ~19.0 and ~19.5 km in Figure 34, is clearly located on the footwall based on the mapped fault strands. It exhibits the lowest elevation of any Bonneville shoreline analyzed in this study, however. Investigation of the lidar in this area indicated that many of the faults are concealed, so there is the possibility that mapped faults could be inaccurate and the shoreline is actually located on a down-dropped hanging wall block. Geologic maps of the area also reveal complex bedrock faults and landslides on the south side of Box Elder Canyon. Deep-seated bedrock landslides or reactivation of bedrock faults can cause block rotation, which would also cause an anomalously low shoreline elevation at this site.

Due to the complexity of both the fault and local geology in this area, we have chosen not to classify shorelines within this complex fault zone as located on the footwall or hanging wall block. Classifications are therefore only made for shorelines with a clear relationship to the main strand of the fault. Because shoreline elevations within the complex fault zone are likely affected by a combination of local geology and activity on the WFZ, we also do not calculate vertical slip rates where shorelines are offset within this zone.

Footwall Elevation Profiles

The majority of the Bonneville and Provo shorelines in this analysis are located on the footwall block of the Wasatch Fault. Therefore, we analyze elevation trends exhibited by footwall block shorelines to interpret fault segmentation patterns because they provide the most comprehensive representation of elevation change along the fault segments (Figure 36). Changes in footwall elevation are not representative of a complete displacement profile, however. Relative uplift along the footwall block of a normal fault is between 10-25% of total displacement on the fault (McCalpin, 2009). Therefore, trends in paleoelevation along the footwall are a low-amplitude representation of the displacement profile for each fault segment.

From the northern boundary of the Brigham City segment (0 km) to the Pleasant View Salient (30 km), the Bonneville shoreline exhibits ~15-20 m in elevation change and the Provo shoreline exhibits ~20 m of elevation change (Figure 36). The northern subsegment of the Brigham City segment exhibits little to no elevation change along the Bonneville and Provo shorelines. Displacement trails off at ~25 km south, just north of

the 60 degree bend in the fault at Brigham City (Figure 36b, Figure 36c). This trend is more evident in the Bonneville shoreline elevations, as the Provo shorelines near Box Elder canyon are heavily modified and not measured in this analysis.

There is no clear decrease in elevation at the Brigham City – Weber segment boundary, which would be expected based on the classic segmentation model. Elevation is relatively constant from the segment boundary south. Shoreline measurements end just north of Bountiful. Shorelines have been heavily modified by anthropogenic activity in and around Bountiful, so it is unclear as to whether displacement decreases at the Weber – Salt Lake City segment boundary.

Vertical Slip Rates

Calculation of vertical slip rates and uncertainties. Vertical slip rates are calculated where the Bonneville and Provo shorelines are offset by the main strand of the WFZ (Figure 37). To calculate shoreline offset, we constrain footwall and hanging wall shoreline measurements to within ~5 km of where the fault trace intersects the shoreline. Offset of the shoreline is calculated as the difference between the mean footwall elevation and mean hanging wall elevation for the ~5 km of shoreline measurements (Figure 38).

Distances greater than ~5 km from where the fault trace intersects the shoreline begin to exhibit trends that would be best represented by a linear regression instead of a mean elevation. The lengths of hanging wall shorelines in all three locations for this analysis are ~5 km or less, however, and a linear regression is less preferable to a mean elevation at this resolution. For this reason, we constrain the footwall elevations to ~5 km

and use mean elevations instead of fitting shoreline measurements with linear regressions. It is important to note here that using shoreline measurements over an area of ± 5 km from the fault trace is a gross estimation of vertical offset, as compared to vertical offsets calculated from piercing points in paleoseismic trenches.

Vertical slip rates are calculated by dividing the mean offset across the shoreline by the known age of the shoreline (Table 3, Table 4). Uncertainty of the slip rate is calculated from combined measurement and shoreline age uncertainties. Measurement uncertainty, measured in meters, is determined from 2 sigma standard deviation (95% confidence bounds) for both the footwall and the hanging wall mean elevations. The total measurement uncertainty is calculated from the root sum squared of the footwall and hanging wall 2 sigma uncertainties. The relative measurement uncertainty, or percentage uncertainty, is the ratio of measurement uncertainty to calculated offset multiplied by 100.

The shoreline ages utilized in this study represent estimated ages from a comprehensive dataset of radiocarbon ages for the Bonneville and Provo shorelines (Oviatt, 2015). Oviatt (2015) does not provide an exact uncertainty, but indicates that an uncertainty of several hundred years is reasonable for these age estimates. We chose an arbitrary uncertainty of ± 300 yr for the Bonneville and Provo age estimates based on this informed opinion (Oviatt, 2015). While this uncertainty is an estimate, like the ages of the shorelines, it serves as a reasonable approximation of the uncertainty associated with the shoreline ages. Relative age uncertainty is then calculated as the ratio of the uncertainty to the age of the shoreline multiplied by 100.

The relative uncertainty of each vertical slip rate is calculated by adding the

measurement and shoreline age relative uncertainties. The absolute uncertainty in mm/yr is then determined by multiplying the vertical slip rate by the percentage of relative uncertainty.

Comparison to Holocene vertical slip rates. The mean preferred vertical slip rates calculated in this study, as a gross estimate of vertical slip, are lower than mean preferred Holocene vertical slip rates calculated from piercing points observed in trenches (Table 5). Uncertainties for the slip rates calculated in this study are large, however, primarily affected by measurement uncertainty in shoreline elevations. Where uncertainty causes the lower bound to be negative, we assign that bound a value of 0 as we do not expect reverse motion on these faults.

The measurements of vertical slip rates on the Provo shoreline at the Pleasant View Salient have the smallest uncertainties for vertical slip rates calculated in this study, so we are most confident in these values. The upper bounds of these slip rates correlate well to the Holocene mean preferred vertical slip rate for the Brigham City segment and the lower bound for the Weber segment.

Vertical slip rates calculated from the Bonneville shoreline at the Pleasant View Salient exhibit lower vertical offset than the Provo shoreline. This measurement challenges the interpretation that as the older shoreline, the Bonneville should exhibit the displacement on the Provo shoreline at a minimum. There is greater uncertainty associated with the elevation measurements on the Bonneville shoreline, however, which at the Pleasant View South location creates a range that overlaps with measurements on the Provo shoreline and Holocene vertical slip rates.

The largest uncertainties are associated with the lowest slip rates located at the

Honeyville Spur. There are no Holocene trenches located this far north along the Brigham City segment with which to directly compare vertical displacement, but the vertical slip rate calculated from the shoreline elevations as compared to the projected Holocene slip rates for the segment are anomalously low.

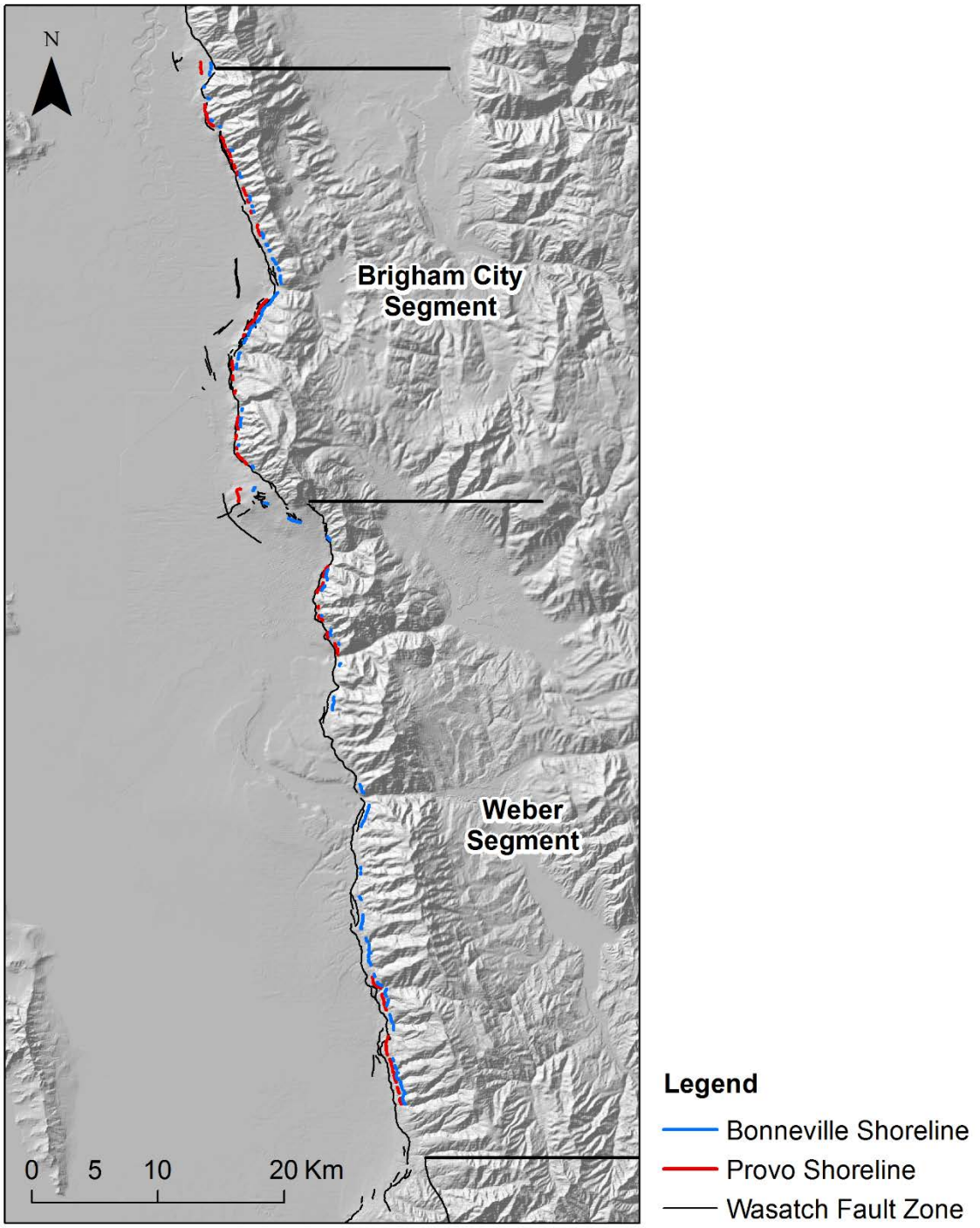

Figure 24. Bonneville and Provo mapped shorelines. These shapefiles were used as input to the PaeloElev tool. Shorelines were mapped to exclude drainages, landslides, alluvial fans, anthropogenic modification, and other factors significantly affecting shoreline morphology.

Table 2. Parameters used in application of PaleoElev to Lake Bonneville shorelines.

1. Inflection Points Script		
Parameter	Value	Description
Profile Spacing	5	Output resolution of 5 m
Profile Length	200	Total profile length of 400 m
Units	"METERS"	Units of profile length
Swath Width	"30 Meters"	Total swath width of 60 m
Statistics Neighborhood	NbrRectangle(40,40,"CELL")	Specified rectangular neighborhood with width 20 m and height 20 m
Edge Effects	3	Width of edge effects in map units (m)
2. Swath Profiles Script		
Parameter	Value	Description
Swath Area	"50 Meters"	Any point within 50 m of the profile is resolved onto that profile
3. Shoreline Elevation Script		
No input parameters required		

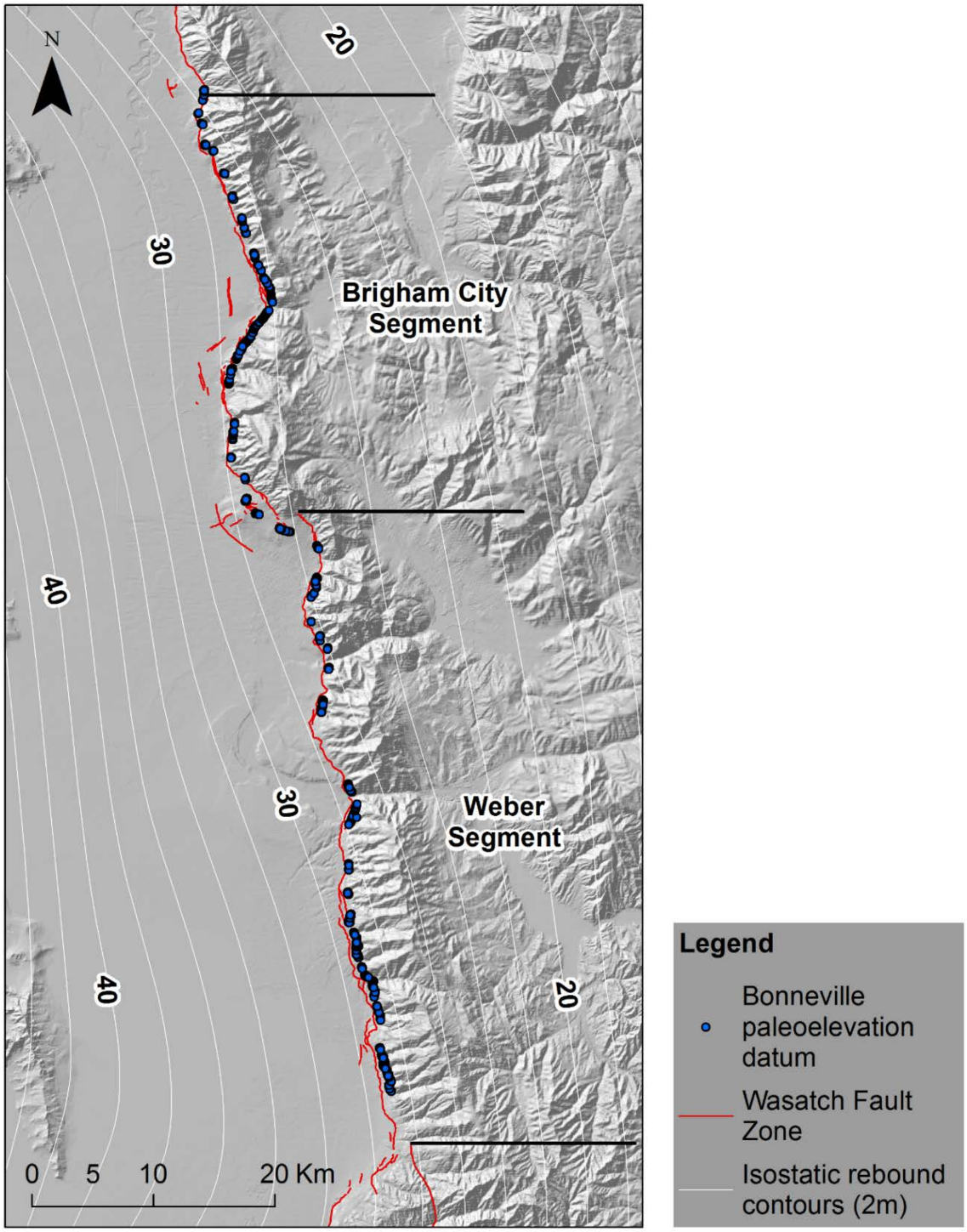

Figure 25. PaleoElev output for the Bonneville shoreline.

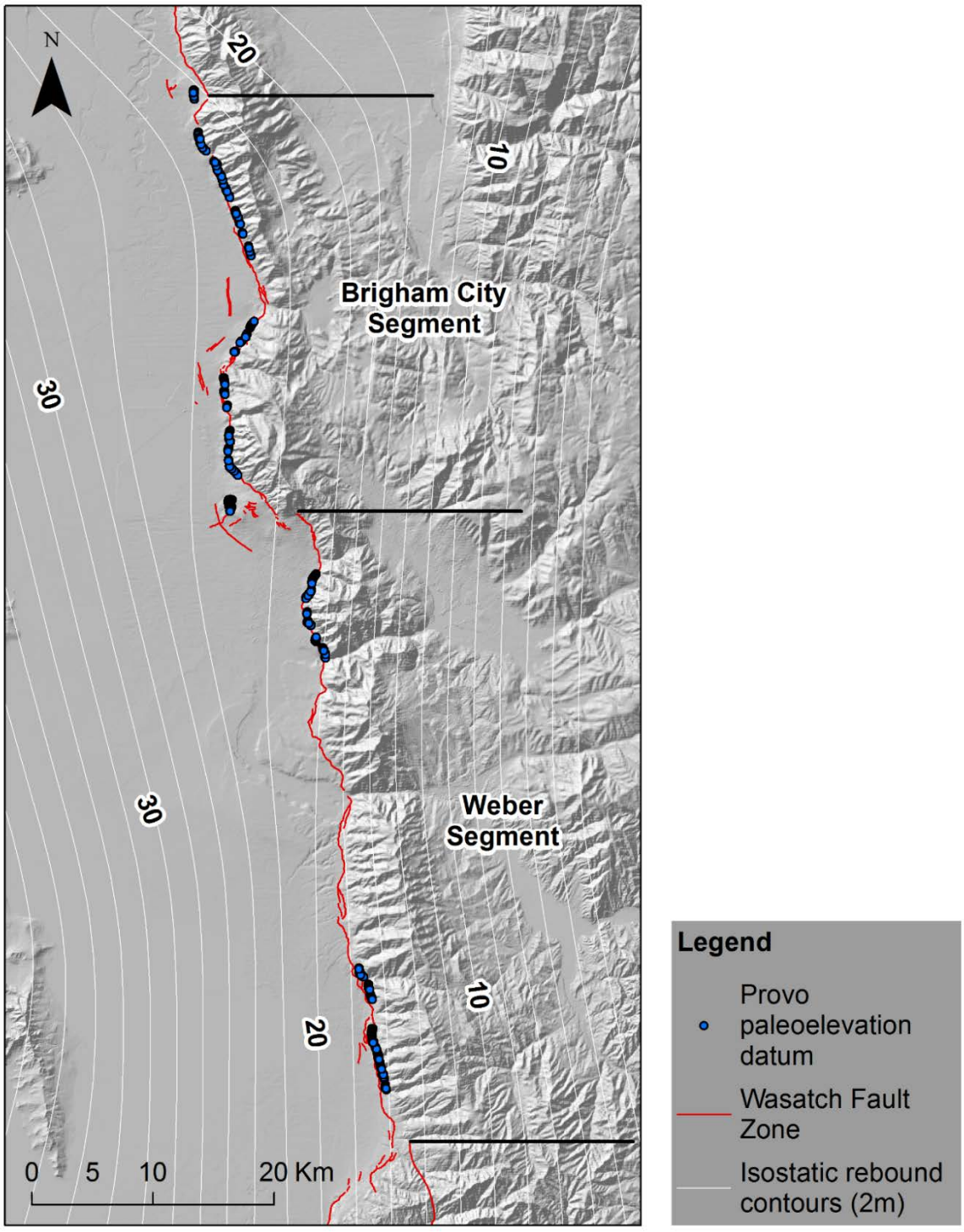

Figure 26. PaleoElev output for the Provo shoreline.

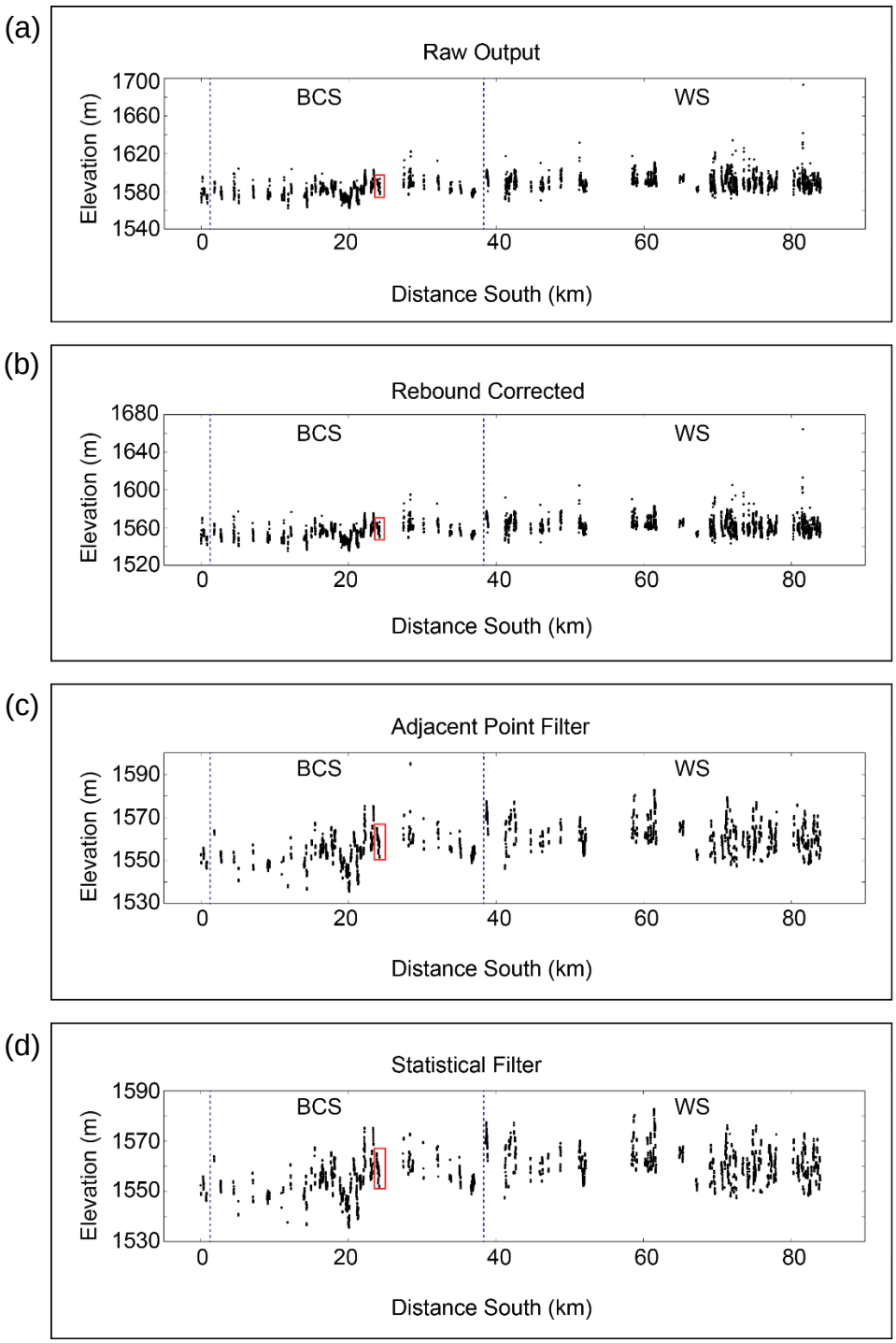

Figure 27. Bonneville shoreline corrections. Paleoelevation datum points are shown in black and the red box indicates the location of Figure 28. Segment boundaries are shown as dotted blue lines, where BCS is the Brigham City segment and WS is the Weber segment. Note the scale change from one figure to the next. a) Output of PaleoElev with no corrections. b) Isostatic rebound correction. c) Paleoelevation datum points meeting the adjacent point criteria. d) Paleoelevation datum points within 3 sigma standard deviations (99.7% confidence interval) for each continuous shoreline section.

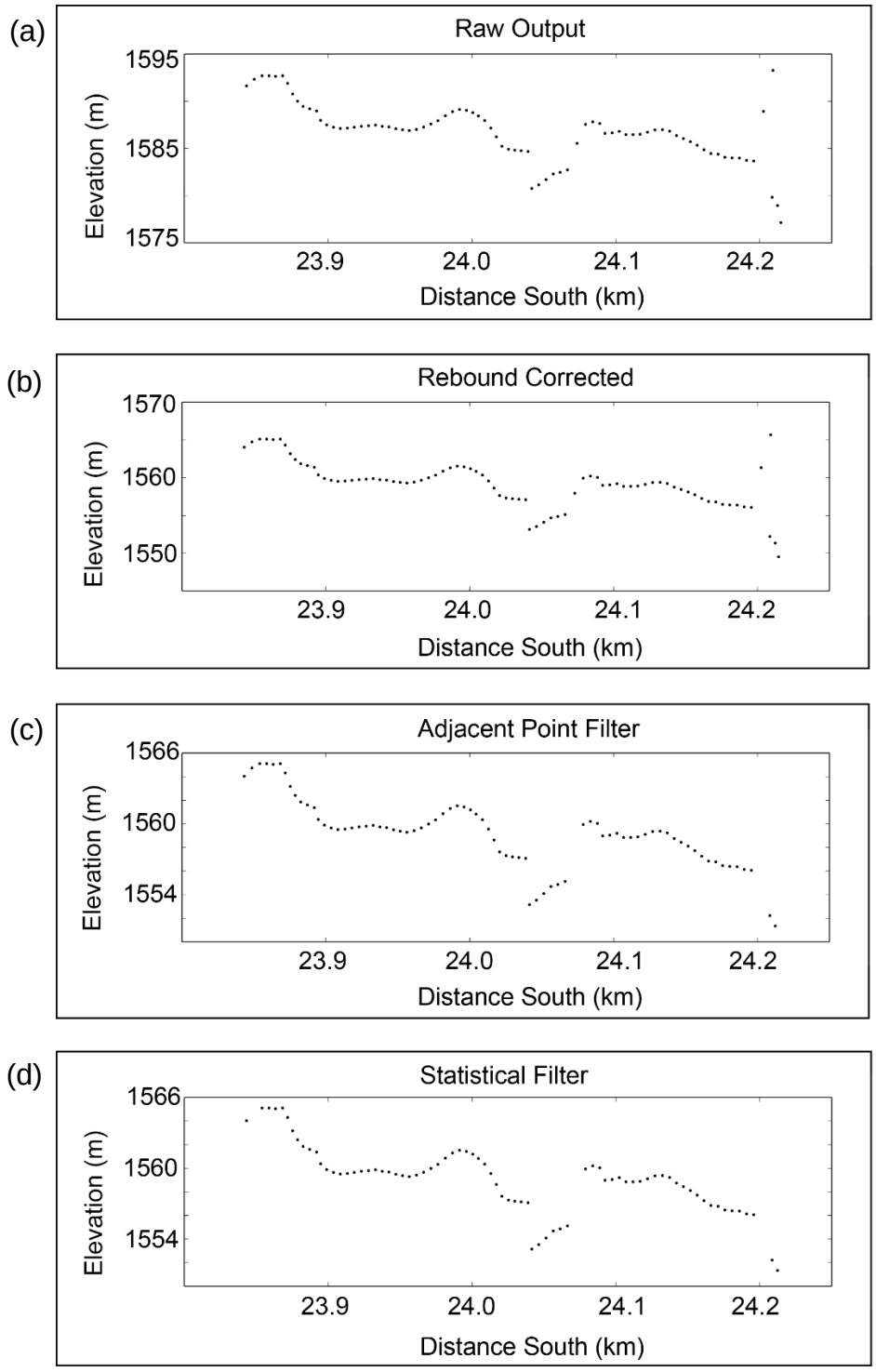

Figure 28. Detail of Bonneville shoreline corrections. Paleoelevation datum points are shown in black. The location of this figure is indicated by the red box indicates in Figure 27. Note the scale change from one figure to the next. a) Output of PaleoElev with no corrections. b) Isostatic rebound correction. c) Paleoelevation datum points meeting the adjacent point criteria. d) Paleoelevation datum points within 3 sigma standard deviations (99.7% confidence interval) for the continuous shoreline section shown.

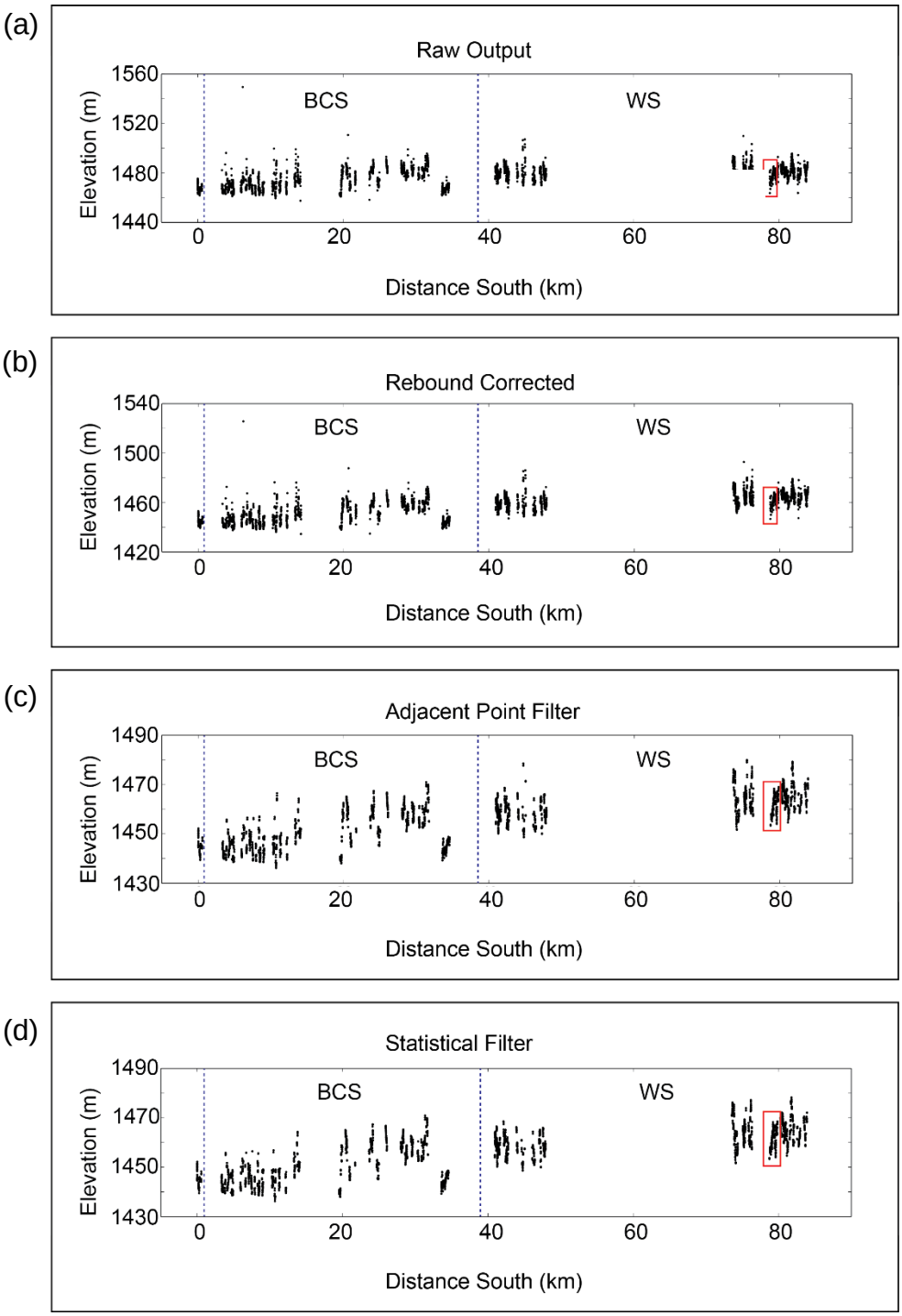

Figure 29. Provo shoreline corrections. Paleoelevation datum points are shown in black and the red box indicates the location of Figure 30. Segment boundaries are shown as dotted blue lines, where BCS is the Brigham City segment and WS is the Weber segment. Note the scale change from one figure to the next. a) Output of PaleoElev with no corrections. b) Isostatic rebound correction. c) Paleoelevation datum points meeting the adjacent point criteria. d) Paleoelevation datum points within 3 sigma standard deviations (99.7% confidence interval) for each continuous shoreline section.

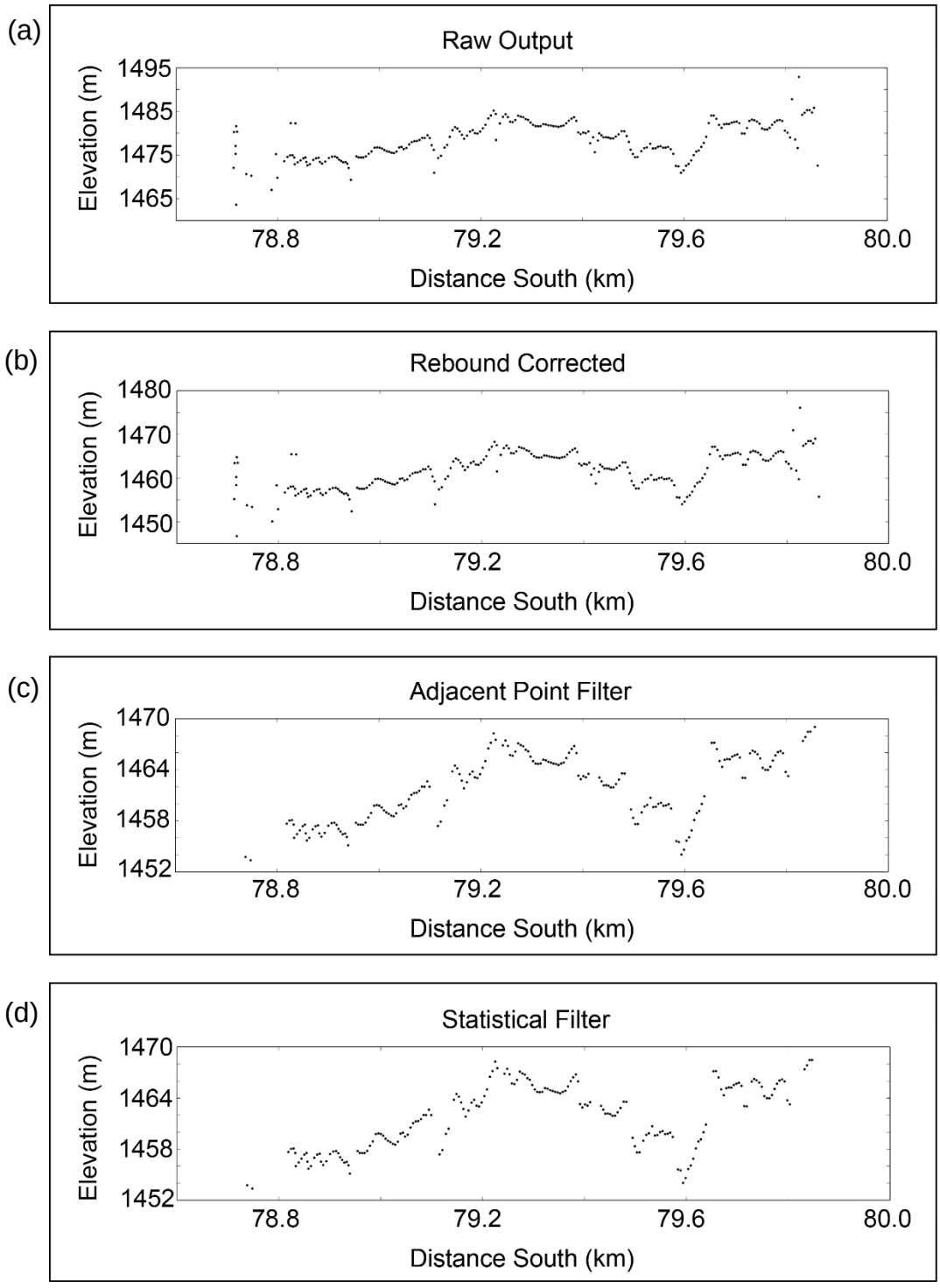

Figure 30. Detail of Provo shoreline corrections. Paleoelevation datum points are shown in black. The location of this figure is indicated by the red box indicates in Figure 29. Note the scale change from one figure to the next. a) Output of PaleoElev with no corrections. b) Isostatic rebound correction. c) Paleoelevation datum points meeting the adjacent point criteria. d) Paleoelevation datum points within 3 sigma standard deviations (99.7% confidence interval) for the continuous shoreline section shown.

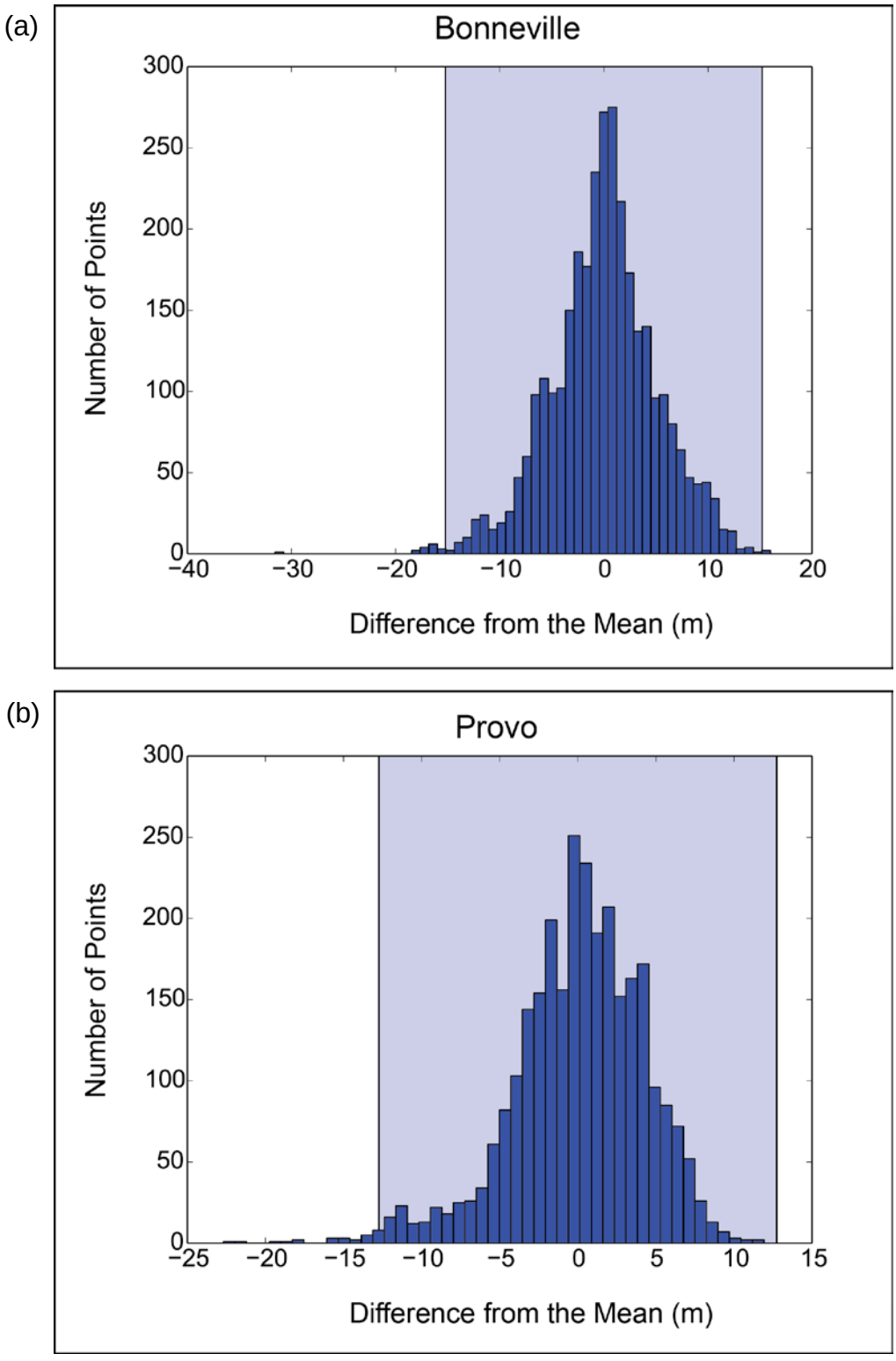

Figure 31. Cumulative distribution of difference from the mean elevation for continuous shoreline sections. The shaded region represents ± 3 sigma standard deviations, which corresponds to a confidence interval of 99.7%. a) Bonneville continuous shoreline distribution. b) Provo continuous shoreline distribution.

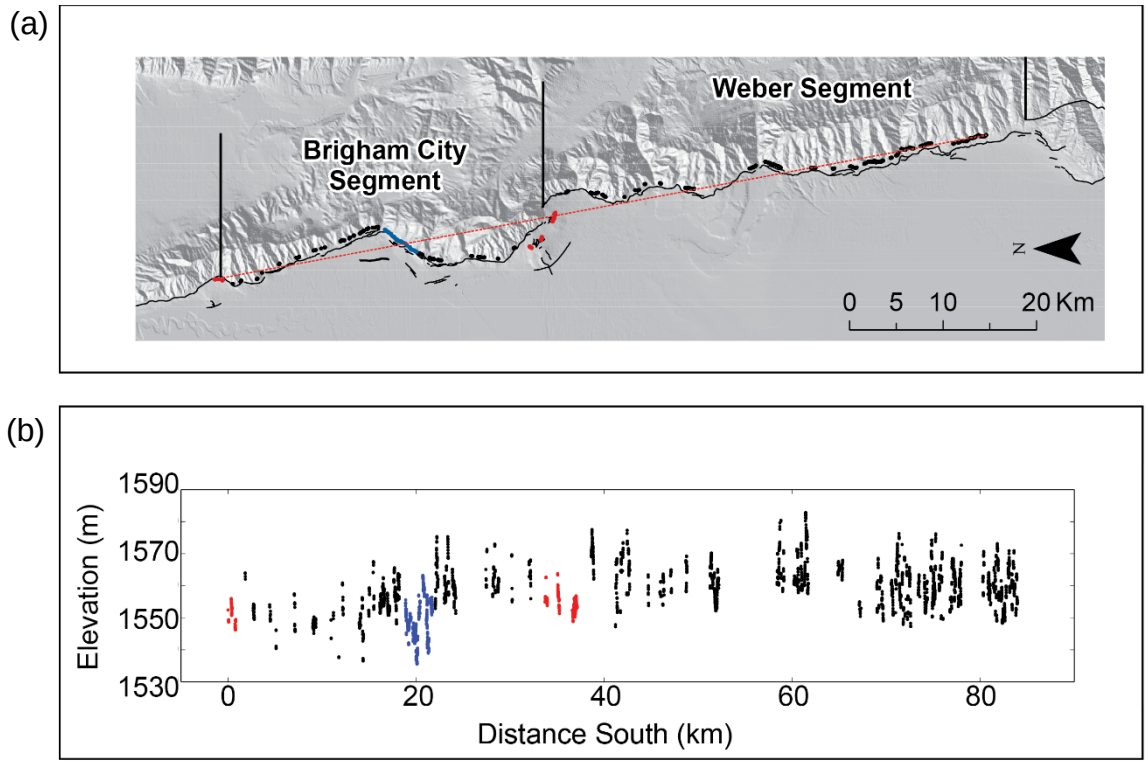

Figure 32. Bonneville shoreline final paleoelevation datum locations and elevation profile. Paleoelevation points located on the footwall of the fault are shown in black and points located on the hanging wall of the fault are shown in red. Blue paleoelevation points represent shorelines affected by complex faulting and geology that cannot be definitively classified as footwall or hanging wall datums. a) Map view location map of final paleoelevation datum points for the Bonneville shoreline. b) Elevation profile of final paleoelevation datum points for the Bonneville shoreline.

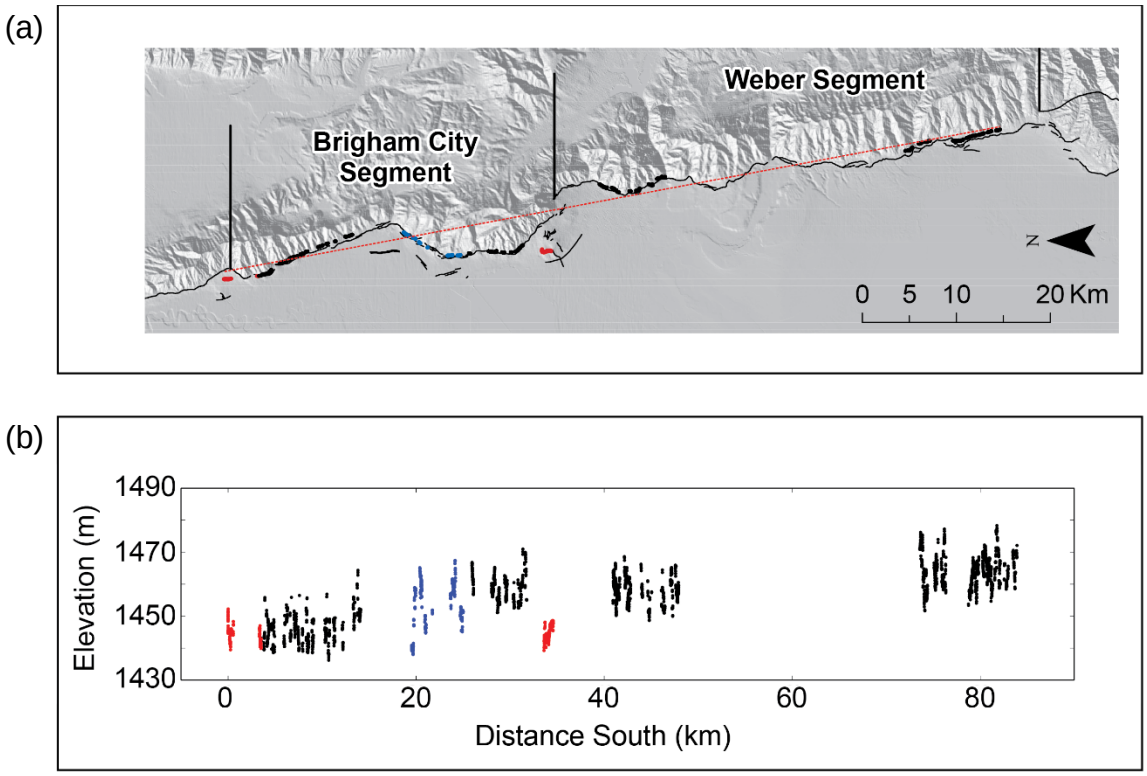

Figure 33. Provo shoreline final paleoelevation datum locations and elevation profile. Paleoelevation points located on the footwall of the fault are shown in black and points located on the hanging wall of the fault are shown in red. Blue paleoelevation points represent shorelines affected by complex faulting and geology that cannot be definitively classified as footwall or hanging wall datums. a) Map view location map of final paleoelevation datum points for the Provo shoreline. b) Elevation profile of final paleoelevation datum points for the Provo shoreline.

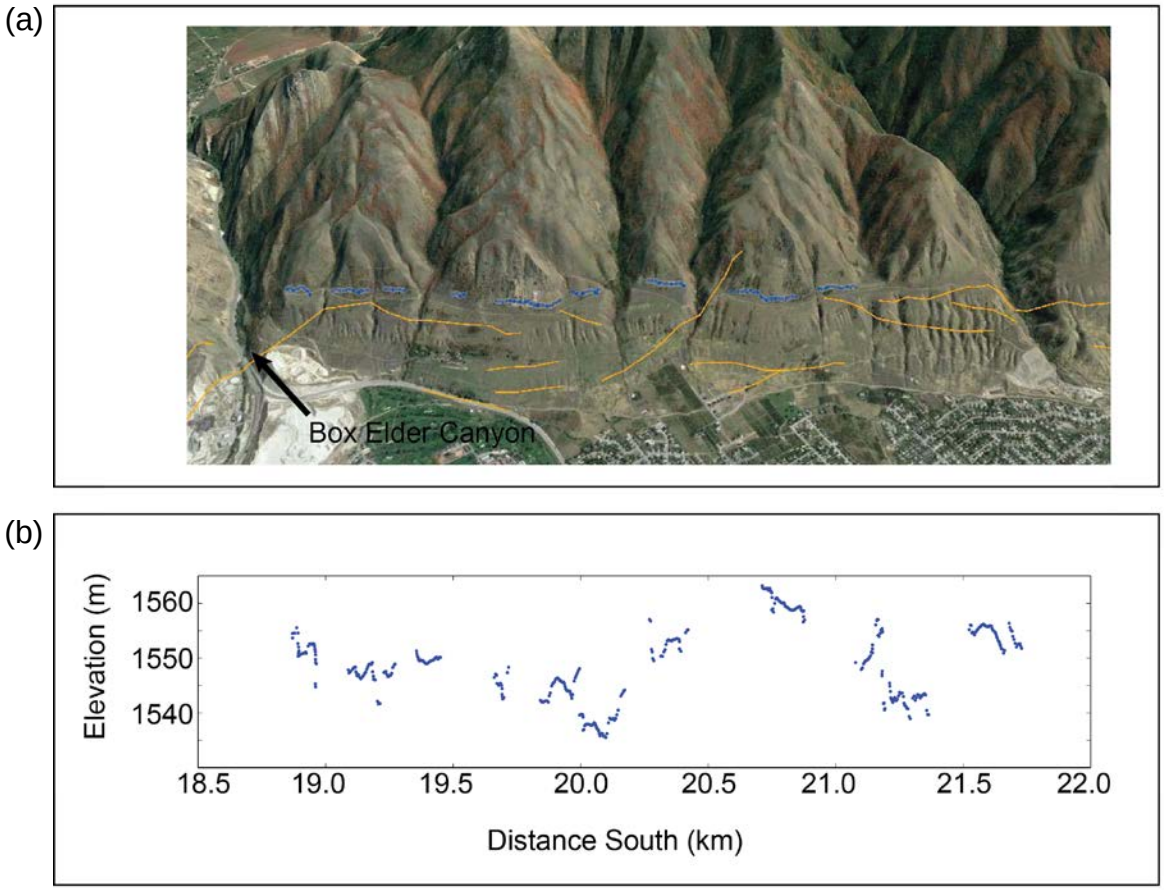

Figure 34. Detail of unclassified paleoelevation datum points on the Bonneville shoreline. a) GoogleEarth image of the local geology, where faults are shown in orange and the location of the paleoelevation datum points are shown in blue. b) Elevation profile for unclassified paleoelevation points.

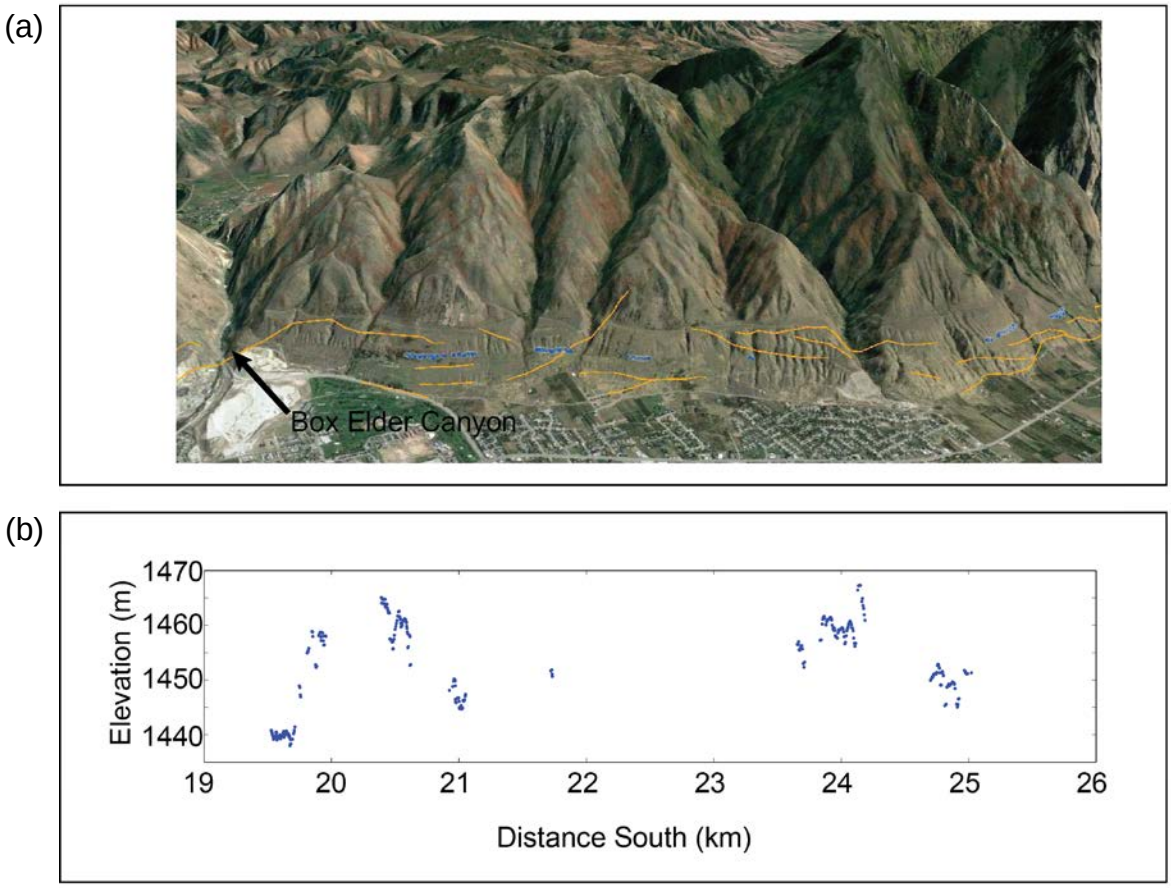

Figure 35. Detail of unclassified paleoelevation datum points on the Provo shoreline. a) GoogleEarth image of the local geology, where faults are shown in orange and the location of the paleoelevation datum points are shown in blue. b) Elevation profile for unclassified paleoelevation points.

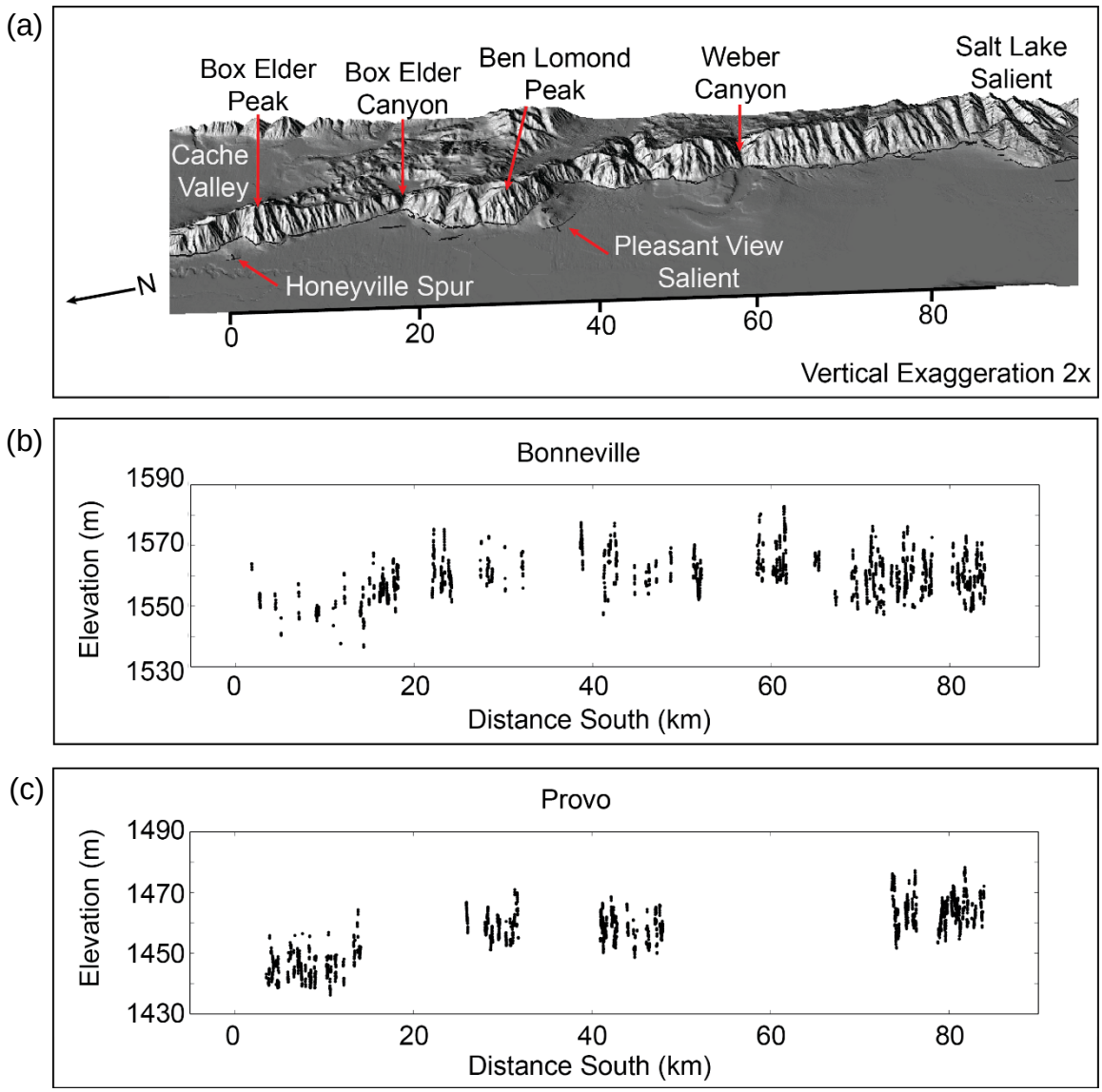

Figure 36. Footwall elevation profiles for the Bonneville and Provo shorelines. Paleoelevation datum points are shown in black. a) Surface topography with significant topographic features labeled. The Wasatch Fault is shown in black. b) Footwall elevation profile for the Bonneville shoreline. c) Footwall elevation profile for the Provo shoreline.

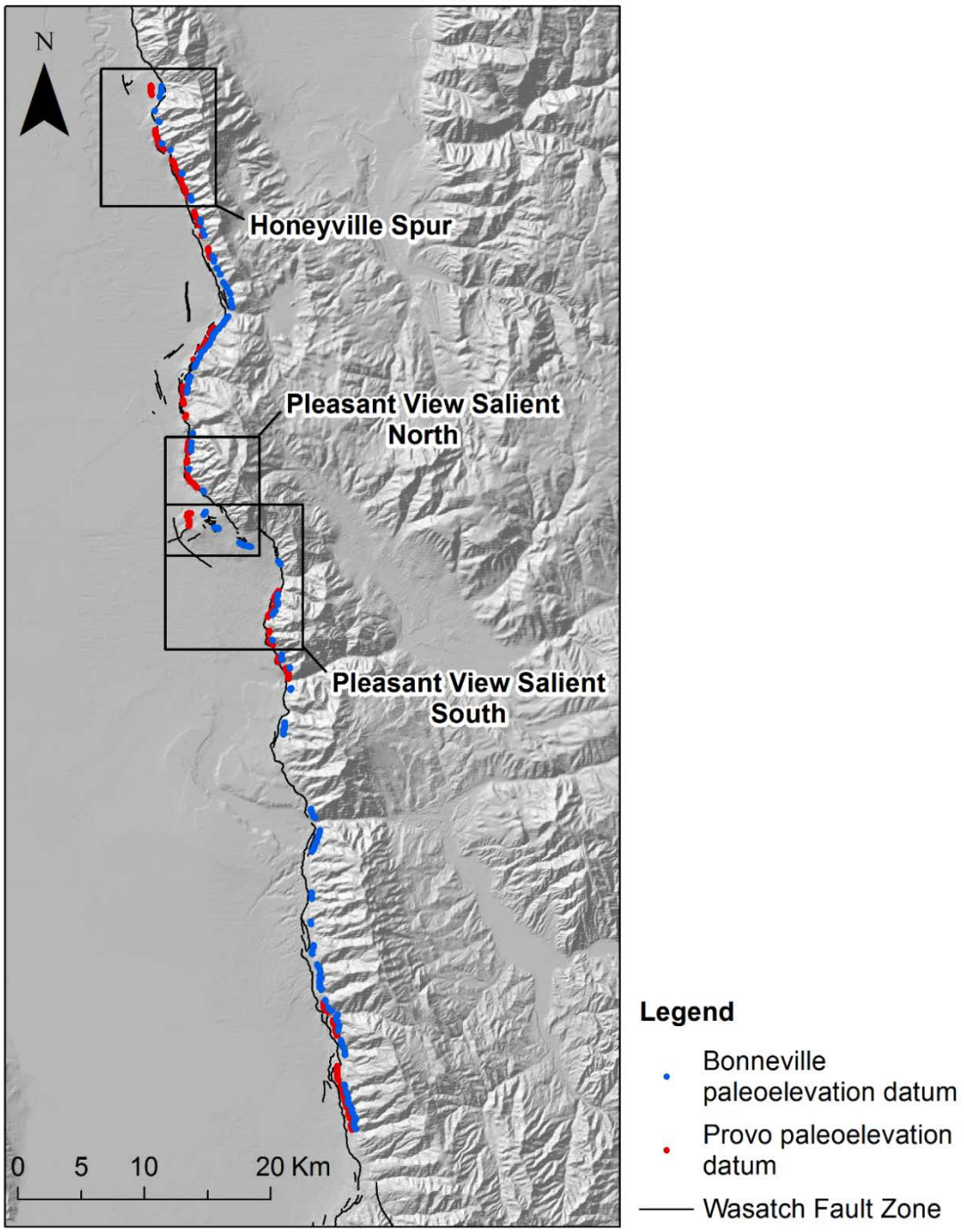

Figure 37. General locations of displaced Bonneville and Provo shorelines.

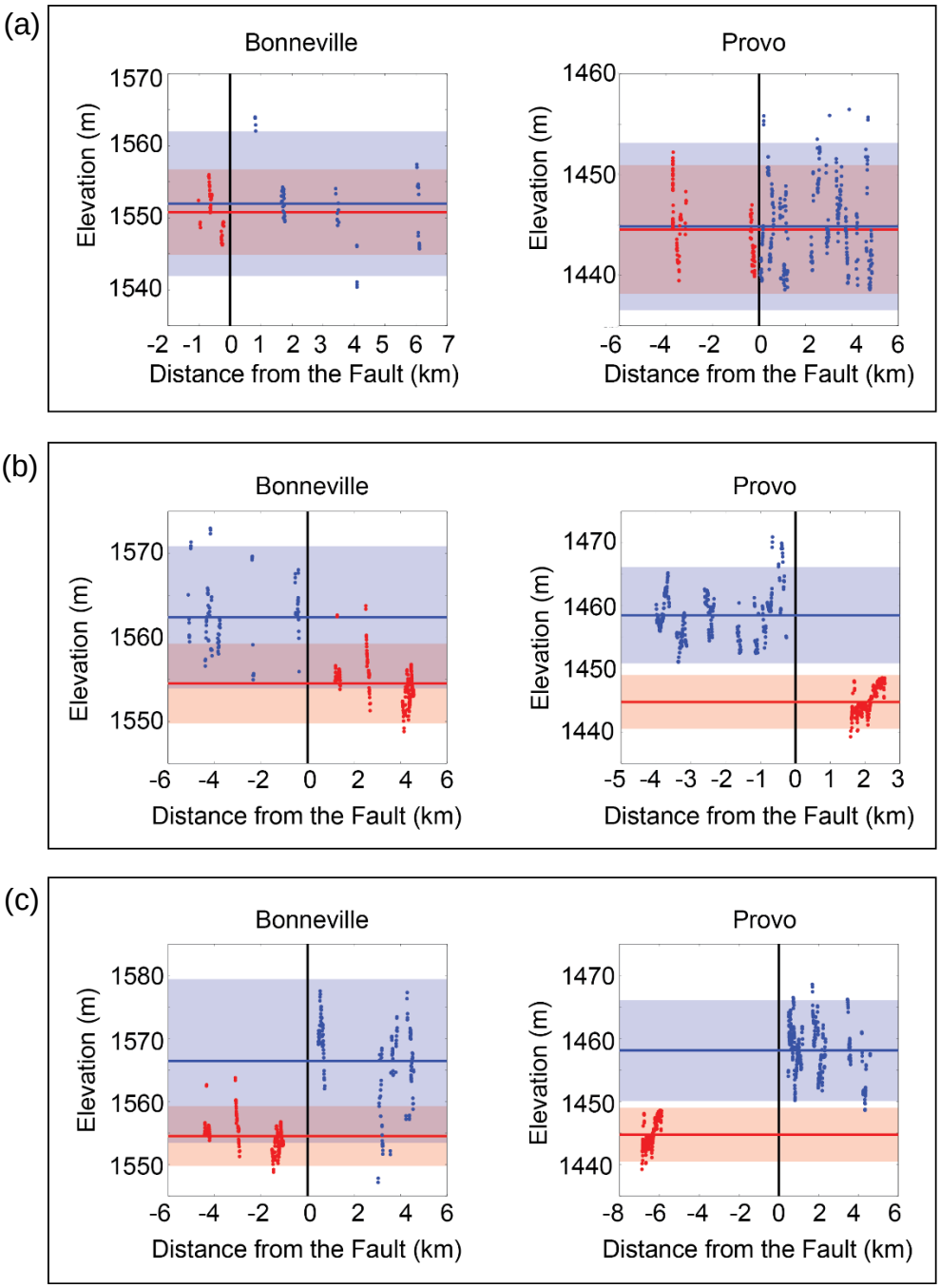

Figure 38. Offset across Bonneville and Provo shorelines. Locations are shown in Figure 37. Footwall paleoelevation datums are shown in blue, where the thick blue line indicates the mean elevation and the blue shaded region indicates a 2 sigma uncertainty (95% confidence interval). Hanging wall paleoelevation datums are shown in red, where the thick red line indicates the mean elevation and the red shaded region indicates a 2 sigma uncertainty (95% confidence interval). The thick black line indicates the location where the fault trace intersects the shoreline, assigned location 0. a) Displacement at the Honeyville Spur. b) Displacement at the Pleasant View Salient North. c) Displacement at Pleasant View Salient South.

Table 3. Bonneville shoreline uncertainties and vertical slip rates.

	Honeyville Spur	Pleasant View Salient North	Pleasant View Salient South
Offset (m)	1.18	7.87	11.91
Hanging Wall 2 sigma uncertainty (m)	5.92	4.71	4.71
Footwall 2 sigma uncertainty (m)	10.01	8.44	12.96
Total measurement uncertainty (m)	11.63	9.66	13.79
Relative Uncertainty (%)	983.76	122.72	115.72
Shoreline Age (yr)	18000	18000	18000
Uncertainty (yr)	300	300	300
Relative Uncertainty (%)	1.67	1.67	1.67
Slip Rate (mm/yr)	0.065	0.44	0.66
Total Relative Uncertainty (%)	985.43	124.39	117.39
Total Uncertainty (mm/yr)	0.079	0.54	0.78
Final Slip Rate (mm/yr)	**0.065 ± 0.079**	**0.44 ± 0.54**	**0.66 ± 0.78**

Table 4. Provo shoreline uncertainties and vertical slip rates.

	Honeyville Spur		Pleasant View Salient North		Pleasant View Salient South	
Offset (m)	0.31		13.76		13.34	
Hanging Wall 2 sigma uncertainty (m)	6.35		4.22		4.22	
Footwall 2 sigma uncertainty (m)	8.27		7.6		7.97	
Total measurement uncertainty (m)	10.43		8.69		9.02	
Relative Uncertainty (%)	3416.92		63.18		67.63	
Shoreline Age Lower – Upper Bound (yr)	15000 - 18000		15000 - 18000		15000 - 18000	
Uncertainty (yr)	300		300		300	
Relative Uncertainty (%)	2	1.67	2	1.67	2	1.67
Slip Rate (mm/yr)	0.02	0.017	0.92	0.76	0.89	0.74
Total Relative Uncertainty (%)	3418.92	3418.58	65.18	64.84	69.63	69.29
Total Uncertainty (mm/yr)	0.7	0.58	0.6	0.5	0.62	0.51
Final Slip Rate Lower Bound (mm/yr)	**0.017 ± 0.58**		**0.76 ± 0.5**		**0.74 ± 0.51**	
Final Slip Rate Upper Bound (mm/yr)	**0.02 ± 0.7**		**0.92 ± 0.6**		**0.89 ± 0.62**	

Table 5. Comparison of calculated vertical slip rates to published Holocene slip rates. Bolded values represent the mean preferred rate, with all values are measured in mm/yr. WGUEP Report values after Wong *et al.* (2016).

	Age	Honeyville Spur	Pleasant View Salient North	Pleasant View Salient South
This Study	Bonneville (18 ky)	0 - **0.07** - 0.14	0 - **0.44** - 0.98	0 - **0.66** - 1.4
	Provo (18 ky)	0 - **0.17** - 0.60	0.26 - **0.76** - 1.26	0.23 - **0.74** - 1.25
	Provo (15 ky)	0 - **0.02** - 0.72	0.32 - **0.92** - 1.52	0.27 - **0.89** - 1.51
		Brigham City Segment		Weber Segment
WGUEP Report (Open mean slip rate per segment)	< 7,000 yr	0.9 - **1.2** - 1.3		1.2 - **1.7** - 2.3

DISCUSSION

Performance of the PaleoElev Tool

Application of the automated PaleoElev tool in measurement of shoreline paleoelevation significantly increased data resolution as compared to previous studies that employed manual analysis. High density shoreline measurements combined with analysis of averaged swath profiles was intended to:

1) Provide a more comprehensive dataset of shoreline paleoelevation along the Brigham City and Weber segments of the WFZ.
2) Reduce surface noise considered a possible cause of scatter in previous studies.

We conclude that these goals for the PaleoElev tool have been met in its application in this study. Although shoreline paleoelevation measurements are more variable than expected, we now have the data resolution to investigate small-scale shoreline variability in detail and are confident that the variability is not derived from the quantitative analysis of the shoreline features.

Aside from meeting its primary functional goals, application of the PaleoElev tool to Lake Bonneville shorelines raised several possibilities for improvements and future applications. Most significantly, outliers produced by the tool as the result of low inflection point densities require more postprocess filtering than initially anticipated. The tool can be updated to include an optional user-defined R^2 threshold in Shoreline_Elevation_Function.py. This new parameter would allow the user to constrain

shoreline output by how well the linear regressions fit the cliff and platform surfaces of each shoreline, likely reducing the need for postprocessing filters.

The speed and processing capability of the PaleoElev tool is currently limited by the use of loops within Python. Python loops are notoriously slow as compared to other programming languages. In addition to being slow, the loops also store data in lists, which can overload the memory of a computer and crash the script if the data files are large. These problems associated with PaleoElev can also be fixed with simple updates. Python allows vectorization of loops, which allows loops to perform at the speed of other programming languages. Vectorization of loops also eliminates storage of data in lists, thereby increasing the speed and reducing the memory needed to process large datasets.

Shoreline Geomorphology

Increased data resolution generated by PaleoElev also provided insight into "scatter" recognized in previous studies measuring shoreline paleoelevation. Regardless of subtle differences in methodology, Meyer and Locke (1986), McCalpin *et al.* (1992), and Jewell and Bruhn (2013) all observed an unexpected amount of variability throughout their shoreline elevation measurements. Explanations for this variability ranged from problems with the methodology to natural variability of the shoreline features. This variability could not be explained in more detail because of relatively low resolution paleoelevation measurements limited by manual profile analysis.

The high-resolution output produced by PaleoElev suggests that variability in these previous studies likely represents a true signal from the shoreline features measured. We propose two possible explanations for the variability evidenced in these

elevation profiles. First, the shorelines could be more heavily modified than is recognizable in lidar and in the field. If this is the case, postformational modification could be a factor contributing to variability. Secondly, these trends indicate that local factors may play a larger role in the formation of basin-wide shoreline features than previously recognized, and as a result, variability of basin-wide correlated shoreline terraces is to be expected.

Our preferred interpretation is that there is likely a combination of these factors causing variability of paleoelevation measurements. We can test this interpretation by comparing shoreline measurements along the Wasatch Front to shorelines in the West Desert, for example, where fluvial and anthropogenic modifications are greatly reduced.

Characterization of Segmentation

Footwall elevation profiles of the Bonneville and Provo shoreline challenge the current characterization of the Brigham City segment. The northern subsegment of the Brigham City segment exhibits little to no vertical offset at the Honeyville spur and nearly constant elevation until it reaches Brigham City. We question, therefore, if the northern subsegment has experienced surface ruptures since the late Pleistocene. The northernmost paleoseismic trenches do not extend to this region (~10 km to ~ 20 km in Figure 36) where we observe significantly reduced displacement along the Brigham City Segment, so there is no Holocene trenching data to compare to the elevations we see along the shorelines.

In contrast, the southern subsegment of the Brigham City segment exhibits elevations approximately equal to elevations along the Weber segment. There is also no

observable decrease in displacement at the Brigham City – Weber segment boundary. This pattern, observed both on the Provo and Bonneville footwall elevation profiles, suggests that the spill-over rupture identified from Holocene trenching data is likely representative of the most probable rupture scenario. The elevation pattern we see across the shorelines on the footwall of the fault indicate that although the southern subsegment of the Brigham City segment and the Weber may have ruptured independently at one time, these segments are now linked and likely rupture coseismically.

Another important observation is that elevation is more or less constant from the southern subsegment of the Brigham City segment to the southernmost extent of our shoreline measurements on the Weber segment. We interpret this elevation signature as evidence for coseismic rupture of the entire segment length as more likely than partial segment ruptures. If partial segment ruptures were more common, we would expect to see elevation minimums along the Weber segment.

We cannot currently make interpretations about the segment boundary between the Weber and Salt Lake City segments. Our shoreline measurements only extend to north of Bountiful, where shorelines have been heavily modified by anthropogenic activity. It is possible that the shoreline elevation decreases as it approaches this segment boundary, as expected based on the classic segmentation model, and this should be investigated further.

Vertical Slip Rates

Vertical slip rates calculated for offset Lake Bonneville shorelines have large uncertainties, primarily associated with the 2 sigma uncertainty of paleoelevation

measurements on the footwall and hanging wall. We interpret this uncertainty not to analytical uncertainty, but true variability associated with shoreline elevation. These large uncertainty ranges complicate our final vertical slip rate calculations, especially where the uncertainty range would cause the vertical slip value to be negative. For example, we can only confidently report the vertical slip rates calculated from the Provo shoreline at the Pleasant View Salient.

Another unexpected observation was that the Provo shoreline exhibited more offset at the Pleasant View Salient locations than the Bonneville shoreline. We propose two possible explanations for the lower vertical displacement on the Bonneville shoreline. First, the morphology of the Bonneville shoreline (a depositional terrace, as opposed to an erosional terrace) complicates precise measurement of paleoelevation, which depresses the tectonic signal. Another possibility is that bedrock faults in the salient, some of which are identifiable in the lidar, in close proximity to Bonneville shorelines on the hanging wall of the fault accommodate some of the displacement from ruptures along the Wasatch Fault. Our preferred interpretation is that preexisting bedrock faults accommodate displacement from ruptures propagating across the Pleasant View Salient.

Anomalously low vertical slip rates at the Honeyville Spur can be interpreted as a decrease in displacement at a known segment boundary. We do not prefer this interpretation, however, based on the elevation profiles of shorelines along the northern subsegment of the Brigham City segment. Instead, we interpret the anomalously low slip rate at the Honeyville Spur as representative of a trend that begins at ~ 15 km south of the Honeyville Spur, where elevation stabilizes at a more or less constant level. We suggest

that the northern subsegment of the Brigham City segment has been significantly less active than the southern subsegment since the late Pleistocene.

CONCLUSIONS

1. The PaleoElev Tool is a useful tool for automated measurement of paleoelevation and can be applied to shorelines and other fluvial terraces in studies of fluvial geomorphology or to neotectonic analyses.
2. The Bonneville and Provo shoreline highstands exhibit variable elevations over short horizontal scales with standard deviations of ± 4.89 m and ± 3.99 m, respectively. This variability may point to local factors as the primary influence in shoreline formation, which can be tested by comparing shoreline measurements from the Wasatch Front to those in the West Desert.
3. Our analysis suggests that the northern subsegment of the Brigham City segment has had little to no activity since the late Pleistocene, as exhibited by a lack of elevation change on the footwall elevation profiles of both the Bonneville and Provo shorelines in addition to a negligibly small slip rate calculated at the Honeyville Spur.
4. The southern subsegment of the Brigham City segment is linked to the Weber segment, and has likely coseismically ruptured with the Weber segment since the late Pleistocene. A lack of decreased elevation at the classically defined segment boundary along the footwall elevation profiles and vertical slip rates calculated at the segment boundary that correspond to mean-preferred Holocene vertical slip rates for the Brigham City and Weber segments support this interpretation.

5. Vertical slip rates have high uncertainties, primarily derived from the 2 sigma uncertainty of shoreline paleoelevation measurements. We interpret this uncertainty as inherent to shoreline variability, not analytical uncertainty, but recognize the complications in reporting vertical slip rates with significant uncertainty. We can further test the precision of the vertical slip rates calculated in this study by comparing them to vertical slip rates calculated on the western side of the Oquirrh Mountains, where Bonneville and Provo shorelines are offset by the Oquirrh Fault but are much less affected by postformational modification.

REFERENCES

Adams, K. D., and B. G. Bills (2016). Isostatic Rebound and Palinspastic Restoration of the Bonneville and Provo Shorelines in the Bonneville Basin, UT, NV, and ID, in *A Scientific Update, Lake Bonneville,* C.G. Oviatt and J. Shroder Jr. (Editors). Elsevier B.V., Chapter 8, 145-163.

Bills, B. G., T. J. Wambeam, and D. R. Currey (2002). Geodynamics of Lake Bonneville, in *Great Salt Lake: An Overview of Change*, J. W. Gwynn (Editor), *Utah Geol. Surv. Spec. Pub.*, Salt Lake City, Utah, 7–32.

Bills, B. G., and G. M. May (1987). Lake Bonneville: constraints on lithospheric thickness and upper mantle viscosity from isostatic warping of Bonneville, Provo, and Gilbert stage shorelines, *J. Geophys. Res.* **92,** 11493–11508.

Bradley, W. C., and G. B. Griggs (1976). Form, genesis, and deformation of central California wave-cut terraces, *Geol. Soc. Am. Bull*. **87,** 553-570.

Chang, W. L., and R. B. Smith (2002). Integrated seismic-hazard analysis of the Wasatch Front, Utah, *Bull. Seismol. Soc. Am.* **92,** 1904–1922.

Chen, C. Y., and A. C. Maloof (2017). Revisiting the deformed high shoreline of Lake Bonneville, *Quaternary Sci. Rev.* **159,** 169-189.

Cooley, S.W. (December, 2014). Perpendicular Transects (Ferreira), in *www.GIS4Geomorphology.com*, Retrieved from http://gis4geomorphology.com/stream-transects-partial/

Currey, D. R. (1982). Lake Bonneville: Selected features of relevance to neotectonic analysis, *U.S. Geol. Surv. Open-File Rept. 2014-1091,* 1–30.

Currey, D. R. (1990). Quaternary paleolakes in the evolution of semidesert basins, with special emphasis on Lake Bonneville and the Great Basin, U.S.A*., Palaeogeogr., Palaeoclimatol., Palaeoecol.* **76,** 189–214.

DuRoss, C. B. (2008), Holocene vertical displacement on the central segments of the Wasatch Fault Zone, Utah, *Bull. Seismol. Soc. Am.* **98,** 2918-2933.

DuRoss, C. B., S. F. Personius, A. J. Crone, S. S. Olig, M. D. Hylland, W. R. Lund,

and D. P. Schwartz (2016). Fault segmentation: New concepts from the Wasatch Fault Zone, Utah, USA, *J. Geophys. Res.* **121,** 1131–1157.

Environmental Systems Research Institute, Inc. (ESRI), (2016). Curvature function, *ArcGIS Desktop Documentation*, Retrieved from http://desktop.arcgis.com

Gilbert, G. K. (1890). Lake Bonneville, *U.S. Geol. Surv. Monograph 1*, 438 pp.

Godsey, H. S., D. R. Currey, and M. Chan (2005). New evidence for an extended occupation of the Provo shoreline and implications for regional climate change, Pleistocene Lake Bonneville, Utah, USA, *Quaternary Res.* **63,** 212–223.

Godsey, H. S., C. G. Oviatt, D. M. Miller, and M. Chan (2011). Stratigraphy and chronology of offshore to nearshore deposits associated with the Provo shoreline, Pleistocene Lake Bonneville, Utah, *Palaeogeogr., Palaeoclimatol., Palaeoecol.* **310,** 442–450.

Hetzel, R., and A. Hampel, (2005). Slip rate variations on normal faults during glacial-interglacial changes in surface loads, *Nature* **435,** 81-84.

Jewell, P. W., and R. L. Bruhn, (2013). Evaluation of Wasatch fault segmentation and slip rates using Lake Bonneville shorelines, *J. Geophys. Res.* **118,** 2528-2843.

Johnson, D. W. (1933). The correlation of ancient marine levels, *Compres Rendus du Congres International de Geographie Paris* **2,** 42–54.

Kern, J. P. (1977). Origin and history of upper Pleistocene marine terraces, San Diego, California, *Geol. Soc. Am. Bull.* **88,** 1553-1566.

McCalpin, J. P. (2009). Paleoseismology in extensional tectonic environments, in *Paleoseismology*, J. P. McCalpin (Editor), *Int. Geophysics Series 95*, Academic Press, London, U.K., 171–270.

McCalpin, J. P., R. M. Robison, and J. D. Garr (1992). Neotectonics of the Hansel Valley–Pocatello Valley corridor, northern Utah and southern Idaho, in *Assessment of Regional Earthquake Hazard and Risk Along the Wasatch Front, Utah*, P. L. Gori, and W. W. Hays (Editors), *U.S. Geol. Surv. Prof. Pap. 1500-G*, Washington, D.C., G1–G18.

Meyer, G. A., and W. W. Locke (1986). Origin and deformation of Holocene shoreline terraces, Yellowstone Lake, Wyoming, *Geology* **14,** 699–702.

Miller, A. A., (1939). Attainable standards of accuracy in the determination of preglacial sea levels by physiographic methods, *J. Geomorphol*. **2,** 95–115.

Olig, S. S. (1994). Seismic hazard evaluation—Kennecott tailings impoundment

modernization project, Magna, Utah, unpublished report, *Woodward-Clyde Consultants* C1-C6.

Oviatt, C. G. (1997). Lake Bonneville fluctuations and global climate change, *Geology* **25,** 155–158.

Oviatt, C. G. (2015). Chronology of Lake Bonneville, 30,000 to 10,000 yr B.P., *Quaternary Sci. Rev.* **110,** 166–171.

Oviatt, C. G., and P. W. Jewell (2016). The Bonneville Shoreline: Reconsidering Gilbert's Interpretation, in *Lake Bonneville: A Scientific Update*, C.G. Oviatt, J. Shroder Jr. (Editors). Elsevier B.V., Chapter 5, 88-104.

Oviatt, C. G., D. R. Currey, and D. Sack (1992). Radiocarbon chronology of Lake Bonneville, Eastern Great Basin, USA, *Palaeogeogr., Palaeoclimatol., Palaeoecol.* **99,** 225–241.

Peacock, D. C. P., and D. J. Sanderson (1991). Displacements, segment linkage and relay ramps in normal fault zones, *J. Struct. Geol.* **13,** 721–733.

Personius, S. F. (1990). Surficial geologic map of the Brigham City segment and adjacent parts of the Weber and Collinston segments, Wasatch fault zone, Box Elder and Weber Counties, Utah, *U.S. Geol. Surv. Misc. Invest. Series Map I-1979,* scale 1:50,000.

Personius, S. F., C. B. DuRoss, and A. J. Crone (2012). Holocene behavior of the Brigham City segment: Implications for forecasting the next large-magnitude earthquake on the Wasatch fault zone, Utah, *Bull. Seismol. Soc. Am.* **102,** 2265–2281.

Pezzopane, S. K., and T. E. Dawson (1996), Fault displacement hazard: a summary of issues and information in *Yucca Mountain Report to the U.S. Department of Energy: Seismotectonic Framework and Characterization of Faulting at Yucca Mountain, Nevada, U.S. Geol. Surv.,* 160 pp.

Schwartz, D. P., and K. J. Coppersmith (1984). Fault behavior and characteristic earthquakes: Examples from the Wasatch and San Andreas fault zones, *J. Geophys. Res.* **89,** 5681–5698.

Walsh, J. J., and J. Watterson (1988). Analysis of the relationships between displacements and dimensions of faults: *J. Struct. Geol.* **10,** 239-247.

Ward, S. N. (1997). Dogtails versus rainbows; synthetic earthquake rupture models as an aid in interpreting geological data, *Bull. Seismol. Soc. Am.* **87,** 1422-1441.

Watterson, J. (1986). Fault dimensions, displacements and growth, *Pure Appl. Geophys.*

124, 365-373.

Willemse, E. J. M., D. D. Pollard, and A. Aydin (1996). Three-dimensional analyses of slip distributions on normal fault arrays with consequences for fault scaling, *J. Struct. Geol.*, **18,** 295–309.

Wheeler, R. L., and K. B. Krystinik (1992). Persistent and nonpersistent segmentation of the Wasatch fault zone, Utah: Statistical analysis for evaluation of seismic hazard, in *Assessment of Regional Earthquake Hazards and Risk Along the Wasatch Front, Utah*, P. L. Gori and W. W. Hays (Editors), *U. S. Geol. Surv. Prof. Pap. 1500*, Washington, D. C., B1–B47.

Wong, I., W. Lund, C. DuRoss, P. Thomas, W. Arabasz, A. Crone, M. Hylland, N. Luco, S. Olig, J. Pechmann, S. Personius, M. Petersen, D. Schwartz, R. Smith, and S. Bowman (2016). *Earthquake Probabilities for the Wasatch Front Region in Utah, Idaho, and Wyoming, Utah Geological Survey Miscellaneous Publication 16-3,* 418 pp.